ΠΑΝΕΠΙΣΤΗΜΙΟ ΘΕΣΣΑΛΙΑΣ
ΠΟΛΥΤΕΧΝΙΚΗ ΣΧΟΛΗ
ΤΜΗΜΑ ΜΗΧΑΝΟΛΟΓΩΝ ΜΗΧΑΝΙΚΩΝ

Computational Aerodynamics Study on the Cooling Effectiveness of Active Brake Ducts for Racing Brake Discs

Alexios Aletras

Υπεβλήθη για την εκπλήρωση μέρους των απαιτήσεων για την απόκτηση του Διπλώματος Μηχανολόγου Μηχανικού

ΒΟΛΟΣ 2023

Η έγκριση της διπλωματικής εργασίας από το Τμήμα Μηχανολόγων Μηχανικών της Πολυτεχνικής Σχολής του Πανεπιστημίου Θεσσαλίας δεν υποδηλώνει αποδοχή των απόψεων των συγγραφέων (Ν. 5343/32 αρ. 202 παρ. 2).

Abstract

Motorsport has always been at the forefront of vehicle development for the last century. Through tough competition, engineers were able to push the technological boundaries of each decade to their limits, to create unique and very special components for race cars, later to be used in road going vehicles as well. Though, what makes a braking system great is the ability to deliver the same braking power repeatedly, during a race around a circuit. One of the key elements of the brake assembly that plays a crucial role in the performance of the vehicle is the brake duct. A brake duct is a specially designed duct that delivers cool air into the brakes, to keep them cool. Brakes lose their ability to stop a vehicle when they heat up to a certain temperature. In this thesis, we examine the advantages of an active brake duct in open wheel racing, which can change the amount of air supply to different areas of the brake assembly, based on their cooling needs. For that purpose, we performed a computational fluid dynamics simulation using ANSYS Fluent software, to determine the aerodynamic and cooling benefits for such a device. We found out that the air supply that is directed to the ventilation channels of a disc brake or the brake pad region can be increased by over 50% and 200% respectively. A race team can program the duct to actively change the air supply to the different components, even during a single lap, maximizing its performance. Brake ducts provide substantial performance and have endless applications in race car design.

Acknowledgements

I would like to thank my girlfriend Serena and my family for their support during the years of my undergraduate study and the writing of this thesis. Also, my close friend George for always pushing me to expand my knowledge of engineering. I would like to thank my thesis coordinator Dr. George Charalampous for providing his expertise and experience in the field of fluid mechanics. Last, but not least, I would like to thank AP Racing for providing the design files of their ventilated, high performance racing brake disc.

Table of Contents

List of Figures

List of Tables

Nomenclature

BBW	Brake-By-Wire
CFD	Computational Fluid Mechanics
COF	Coefficient of friction
DNS	Direct Numerical Simulation
ECU	Electronic Control Unit
LES	Large-Eddy Simulation
MGU	Motor Generator Unit
NS	Navier-Stokes (equations)
PIV	Particle Image Velocimetry
RANS	Reynolds Averaged Navier-Stokes Equations
Re	Reynolds number
Wake	The fluid effects occurring behind an object
Disc Eye	The inner opening of the disc rotor which directs the air to the ventilation channels

1. Introduction

1.1 Development of disc brakes and brake cooling

Brakes are a very important component of a vehicle, whether it is an ordinary road car or truck or a race car. The brakes used today are based on a hydraulic braking system. This means that a fluid is used to deliver the energy from the driver's foot to the actual braking unit, either the brake disc or the drum brake. When the driver presses the brake pedal, brake fluid is pressurized in a cylinder. That cylinder is called a master cylinder and is connected with a fluid reservoir and brake lines, which deliver the pressure to all four wheels. The braking mechanism is housed either in a caliper for disc brakes or a drum for drum brakes.

Drum brakes are a type of brake that uses the friction between the brake lining and drum to stop the vehicle. They consist of a drum, which rotates with the wheel, a brake cylinder which provides the braking pressure, two brake "shoes" or pads which contain the brake lining and press onto the drum to slow down the vehicle.

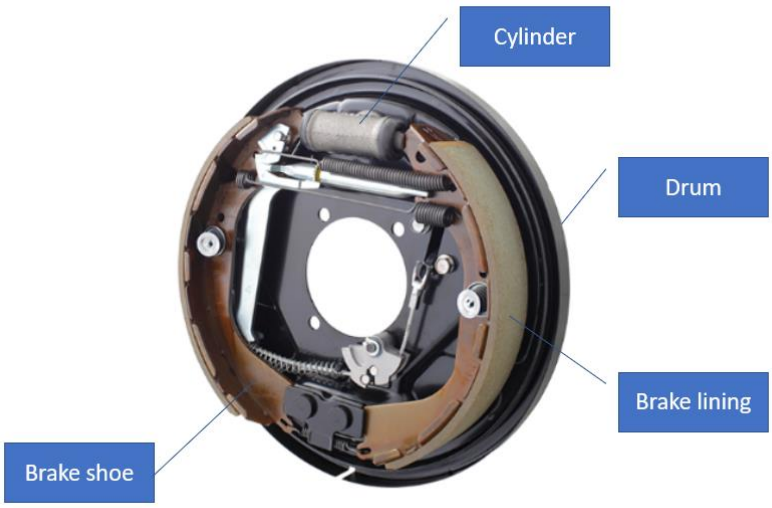

Figure 1 Drum brake.

Disc brakes use the friction between the pads and brake disc to slow down the vehicle. The whole assembly is housed in a caliper, usually made from cast iron, or forged steel. Inside the caliper a piston or in some cases, multiple pistons distribute the pressure of the brake fluid to the pads and then on the disc surface. A multiple piston design may be used for a more evenly distributed braking

force on the disc. Disc brakes are the universally preferred braking system when it comes to sports cars and racing cars, mainly for their cooling characteristics. Drum brakes cannot dissipate the generated heat as quickly as disc brakes and may suffer from thermal and mechanical distortion, due to the high temperatures (Day, 1987). This thesis will focus solely on the development of disc brakes since it is the most used type of braking system in racing. During braking, a large amount of energy is produced in the form of heat. The main source of that energy is the friction between the brake disc and brake pads. A simple schematic of the braking system of a passenger vehicle is shown below. As the driver presses on the brake pedal, a pushrod moves a piston in the master cylinder which is connected to brake lines, delivering pressure to the front and the rear of the vehicle. The pressure of the brake fluid will in turn, push the pistons on the brake caliper towards the brake disc, creating friction and slowing down the vehicle.

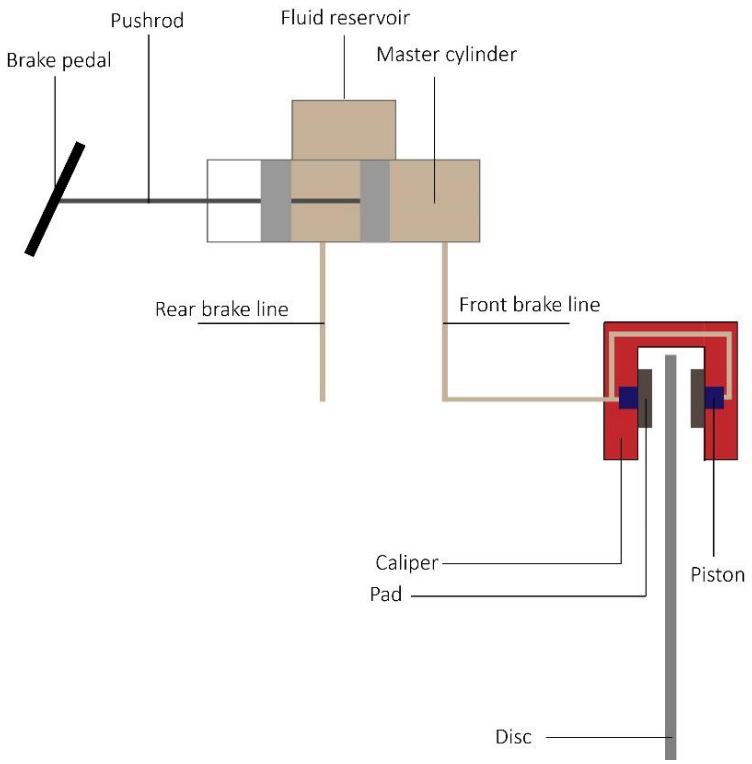

Figure 2 Disc brake system assembly diagram

When the driver applies the brakes, the kinetic energy of the vehicle is converted into thermal energy, significantly increasing the temperature of the brake discs and other components. Experiments have shown that even a braking period of 5 seconds on a road car can increase the surface temperature of a brake disc more than 500°C (Adamowicz and Grzes, 2011). This is to be expected;

thus, the braking system of a vehicle is designed according to the vehicle's braking and cooling needs. When the temperature increases the coefficient of friction is typically observed to decrease significantly, over a relatively narrow range of temperature, commonly referred to as, the transition temperature (Pearson *et al.*, 2013). Below we are able to observe such an example for a material commonly used in brake discs. The phenomenon of overheating brakes is now of a great importance in vehicle safety.

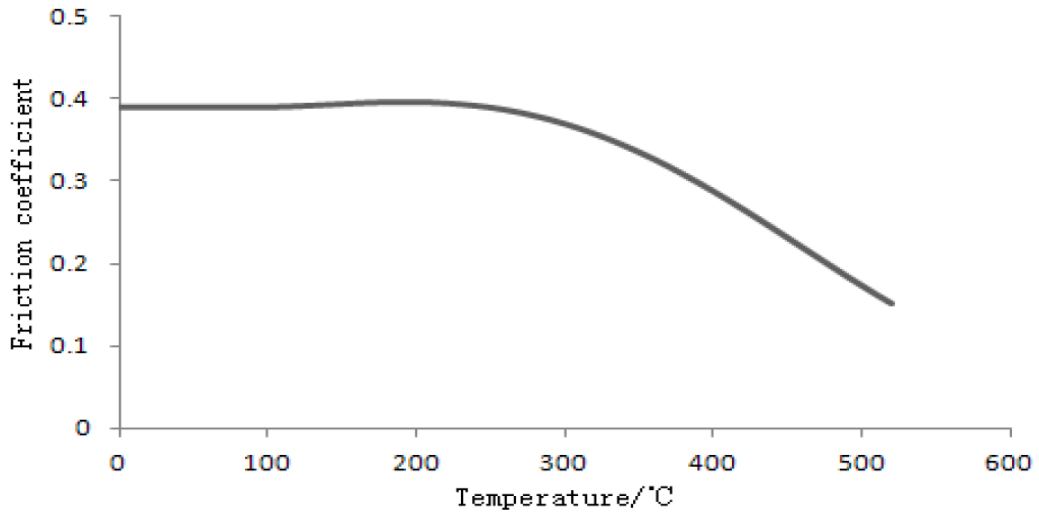

Figure 3 Time- friction factor curve of HT250 cast iron. (Zhang and Xia, 2013)

If the breaks overheat, their braking capability drops considerably, due to the decrease of the coefficient of friction (COF) of the brake pads and disc. This phenomenon is called brake fade. The COF is a dimensionless number which relates the normal force and the friction force of two contacting surfaces. High temperatures during braking, may cause brake fade, premature wear, brake fluid vaporization, bearing failure, thermal cracks, and thermally excited vibration (Valvano and Lee, 2000). Premature wear is caused when the friction material of the brake pads wears off more quickly than designed. Brake fluid vaporization occurs by the radiation emitted from the overheating brakes, heats the brake lines. Bearing failure means that the hot bearing lubricant breaks down and can cause scoring and etching of the bearing surfaces. In road cars, brake discs are made from cast iron and should not exceed 600°C, otherwise the vehicle will experience brake fade. Also, after repetitive braking, the brake fluid's temperature increases, especially during the "heat soaking" period or when the car is finally stopped (Lee, 1999). When a car is being used, inevitably, water will enter the brake lines. This will increase the water content of the brake fluid, which has a significant effect on its performance. More specifically, when part of the brake fluid vaporizes, the whole hydraulic braking system loses its effectiveness. Water content plays a major role in the

phenomenon, as shown in the figure below.

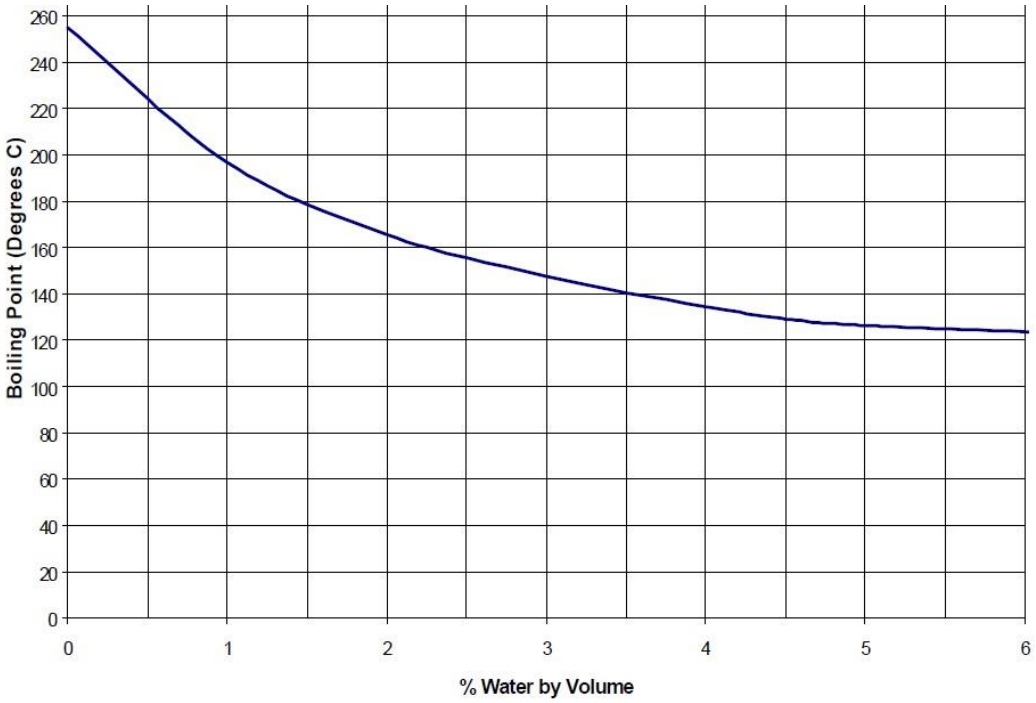

Figure 4 Boiling point vs. water content of DOT (USA Department of Transportation) 3 brake fluid

As the water content increases, the boiling point of the brake fluid decreases, resulting in a much higher chance of having performance issues. That is why in road cars it is important to change the brake fluid after the recommended usage time. Especially in the case of high-performance road cars since they will probably be used in racetracks or be driven aggressively on demanding roads. In racing though, although high-end brake fluids are being used (such as the MOTUL RBF 660) that can provide a dry boiling temperature of 325°C, water content never plays a big role since racing teams frequently change the brake fluid in their cars.

The stopping capability of a brake increases with the rate at which heat is dissipated due to forced convection and thermal capacity of the system (Belhocine and Wan Omar, 2018). Clearly a need for effective brake cooling is necessary to ensure vehicle safety but, another reason for effective cooling, would be to increase the performance of the vehicle.

This is usually not an issue for ordinary road cars, because the cooling from the ambient air flow is normally sufficient, considering the heat generation rate during driving. A more advanced cooling system would not make a big difference in the performance of the car. Sports cars and race cars on the other hand, have higher performance and are more likely to be used for racetrack driving and similar conditions that places a higher demand on the brakes. In motorsport, carbon brake discs are

used to increase performance. They can reach temperatures up to 1000-1200°C and still be able to deliver their braking capabilities. At these temperatures though, the phenomenon of thermal oxidation should be taken into consideration. The oxidation of the carbon matrix and fibers of the brake disc also affects the fiber-matrix interface and weakens the overall integrity of the composite (Bevilacqua, Babutskyi and Chrysanthou, 2015). Convection is the most important mode of heat transfer, dissipating the highest proportion of heat to surrounding air in most vehicle operating conditions. Conduction is the least studied mode of heat transfer, whereas radiation significantly contributes to heat dissipation at high temperatures (Voller *et al.*, 2003). The first brake discs to be used lacked the ventilated channels which increase convective cooling, so in the 1950s the first ventilated discs were installed in a car. The American Crosley Hot Shot, for six months in 1950, built a car with ventilated discs and in 1951 in Formula One racing, one of the BRM Type 15s used a Girling produced set.

Figure 5 Ventilated disc with integrated (non-floating) mounting bell. Image courtesy of AP Racing

Above, we see a ventilated disc with a mounting bell as one piece. This kind of design can be found mostly in road car applications because it is simple and cheap to make. In order to save weight and allow the disc to expand in both radial and axial directions, a floating mounting bell is used in motor racing. Such an example can be shown in the figure below.

Figure 6 Ventilated disc with floating mounting bell. Image courtesy of AP Racing

Mounting bells are usually made from aluminum alloys and provide a lighter solution to the brake assembly. A mounting bell can be attached to the disc either with a bolted or a “floating” method. The first one provides a sturdier assembly and is mainly used for heavy duty applications, such as off-road racing. The second one, utilizes bobbins to allow radial and axial “float”. What this means is when the disc reaches high temperatures, it expands both radially and axially. Without the “float” distance, which is usually 4 to 5 tenths of a millimeter, the disc would experience thermal distortion and a higher chance of rotor coning. Rotor coning causes the contact surface between the brake pads and the rotor to bend and thus not being parallel to the wheels, creating uneven braking and stress loads (Valvano and Lee, 2000).

Flow analysis and heat dissipation of disc brakes have fascinated many researchers. Some of the earlier work includes the analysis of the aerodynamics of disc brakes, (Hudson and Ruhl, 1997; Jerhamre and Bergström, 2001; Johnson, Sperandei and Gilbert, 2003) and heat transfer (Valvano and Lee, 2000; Voller *et al.*, 2003). Hudson and Ruhl concentrated on design modifications to improve the vane flow on the flow inlet conditions, of a ventilated disc. They experimented with various inlet designs and measured a 3-6% decrease in surface temperature at the end of a ten stop fade test. (Jerhamre and Bergström, 2001) measured the correlation between CFD and experimental analysis of a flow field of a ventilated disc. The CFD data obtained underestimated the tangential velocity by 4% and the radial velocity by 14%. Johnson, Sperandei and Gilbert used *Particle image velocimetry* (PIV) to measure air velocities through the air passages of an automotive ventilated disc. They found that

the areas with the highest turbulent kinetic energy occurred through the middle of the air passages. Also, by using normalized mean velocity plots they found little variation at the three rotational speeds tested, indicating a linear relationship between the velocities established in the rotor and rotational speed. Valvano and Lee performed a finite element-based thermal stress analysis to calculate the thermal stress and distortion in a disc brake during a series of braking actions and compare them with measured data. Voller and his colleagues used a spin rig to study all the three modes of heat transfer (conduction, convection and radiation) and he performed a finite element method to compare the results. He found that the experimental results correlated with the numerical ones, making the test spin rig a valuable piece of equipment for future tests.

In the recent years, further development of the materials and components of the braking systems in racing meant a new way of cooling the brakes was needed. The last decade saw the development of brake ducts. Brake ducts are specially designed ducts that channel air into the brakes in order to improve the cooling.

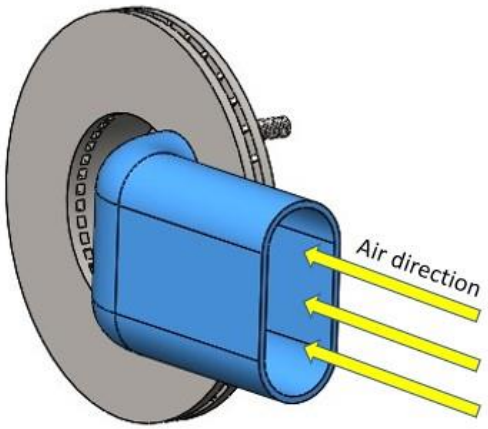

Figure 7 Brake duct assembly

There are numerous ways to design a brake duct regarding the inlet and outlet position thus, deciding what specific component of the brakes will be affected. They are relatively inexpensive to make and versatile and do not experience any significant wear during use. Not many studies have been conducted on brake ducts with one of a few examples being the study by (Jeong *et al.*, 2014a). Parameters such as direction, location, shapes, and the size of the duct, were put to the test. Results showed that the optimal direction of air is towards the vane inlet of inner disc side and the angle is the most adjacent without interference of tire.

Another type of brake cooling is liquid brake cooling. Although it has not caught on with the racing standards, water cooled brakes have been used in rally racing providing a higher temperature

drop on caliper temperature compared to air cooled systems. But the idea of a liquid cooling system was quickly discarded as it added extra weight to the calipers and would be extremely unsafe in a case of a pump breakage.

As of today, the best performing and mainstream method of brake cooling in sports and race cars is the use of a brake duct. By creating air channels, engineers can easily direct the air where necessary and increase the convective cooling of the brake disc and pads. Another advantage of brake ducts is that they are easy to develop through Computational Fluid Dynamics (CFD) and then validate the results in a wind tunnel or on the track.

The main limitation of brake ducts is their size. They must be big enough to channel the required supply of air into the brakes to achieve the heat dissipation needed, but small enough so that their interference with the air flow is at a minimum. Generally, brake duct inlets need to have a clear view of the incoming air flow. This is achieved with cutouts in the front bumper and grill in road cars and race cars and then channels direct the air to the brakes but at the same time the aerodynamic drag of the car is increased. In open wheel racing the duct, is mounted directly on the upright of the suspension resulting in a more compact design. In this case not only is drag increased but, the air flow that follows the duct is now compromised. A duct with a small inlet diameter would help minimize the effect on the aerodynamic performance of the vehicle but the risk of insufficient cooling would be considerable.

This thesis will examine the further development of the brake duct concept through CFD. More specifically a number of duct designs will be developed in order to be used on a ventilated brake disc and improve its cooling. The main purpose of the duct will be to increase the convection cooling of the ventilation channels by directing the air towards them. Another purpose of the duct will be to supply the brake pad area with cooling air to achieve better heat dissipation. Firstly, different duct designs will be produced, in order to test different layouts and approaches. For the second stage of the analysis, a CFD simulation driven comparison of all the different designs will take place, from which the best design will be selected. The objective is to increase the air velocity either in the ventilation channels or the brake pad region. Also, the aerodynamic effects of an active brake duct design will be considered. The computational method will simulate the working conditions of a brake duct in an open wheel racing format at high speeds. Finally, the thesis will examine the further development of brake ducts and more specifically active brake ducts. An active flap will be installed in the duct, creating channels within the duct with the purpose of cooling different parts of the brake assembly. By changing the inlet surface area (i.e. the angle of the flap), air can be directed where it is most needed, for example 100% to the disc channels or 80% to the disc channels and 20% to the brake pads. Finally,

the duct angle, otherwise the angle of the air jet in relation to the disc surface, will also be taken into consideration. The different designs will include angles of 50°, 60°, 70°, and 90°.

1.2 Racing braking system

In race cars, the braking system is a bit different from road cars. When the driver steps on the brake pedal, it compresses two separate master brake cylinders - one for the front wheels and one for the rear - which generate fluid pressure. On road going vehicles only one master brake cylinder is used. For safety reasons, in racing they use two and each master cylinder provides a separate supply of brake fluid from separate reservoirs, so in case of brake failure, the car will be almost controllable with just the front or rear brakes working.

In recent years, many racing series have developed a hybrid or fully electric unit such as Formula 1 and Formula E. The braking system for this type of vehicles is different compared to the system described above.

At the front, the system is like the one used in road cars. The fluid pressure is delivered directly to the front brake calipers, bringing the brake pads and brake disc in contact and this is how braking occurs at the front. At the rear, there are three ways to decelerate the wheels: using the disc brakes, "engine braking", which occurs when the driver is not pushing the accelerator and coasts the vehicle and finally, electrical braking that results from harvesting energy by the hybrid electric motor - the MGU (Motor Generator Unit). An MGU motor is used in many road going vehicles nowadays, that implement a mild hybrid, plug-in hybrid, or full electric powertrain. An MGU is an electromagnetic motor that generates electric energy from the kinetic energy of the wheels, resulting in the retardation of the rear wheels. That energy can be used to recharge a battery for the hybrid or electric unit and then via the MGU, be delivered back to the rear wheels.

In racing, the driver has full control of the energy harvesting system and all other ways of braking the front and rear wheels via the Brake By Wire system (BBW). If the driver applies the brakes into a corner, he expects the same braking results every lap, assuming he applies the same force onto the braking pedal. With the above three systems, only by disc we can accurately predict the braking force, whereas with the other two, (engine braking and electric braking), the deceleration may vary. Engine braking depends on the rpm of the engine and this value may be different every lap. Electric braking can be adjusted by the driver using the buttons on his steering wheel, depending on his energy deployment needs throughout the lap or race. The BBW system ensures that every time the driver presses the pedal with a given force, the braking result will be the same, to ensure maximum performance.

The BBW system is a control system consisting of the brake pedal (signal), pressure sensors, the electronic control unit (ECU), and the front and rear braking systems. The signal, i.e. the overall braking force required by the driver is processed by the ECU, which then, applies each braking system accordingly. This action can be further modified by the team for better braking performance, according to the setup of the car for any circuit, or the driver via his steering wheel. An example of the modifications that can be implemented is the adjustment of the brake bias between the front and rear wheels.

As previously mentioned, brake cooling in racing is one of the most important areas of a car's design. The system described above, although complex, is based on a very simple principle. Keeping the disc and pad temperatures inside their working range. Brake ducts are the best solution we have to satisfy the cooling needs of a race car but from an aerodynamic perspective, there is room for improvement. The BBW system coupled with an active brake ducts system will satisfy both the cooling and the aerodynamic needs of the vehicle, without any significant increase in the cost, since all the hardware is already present. The active brake ducts can be part of the control system and according to the readings of the temperature sensors, the system will be able to close or open the duct inlet, increasing the vehicle's performance.

1.3 Calculating braking power

For the total braking power

$$P_{tot} = (F_F + F_R)U + F_D U \quad (1)$$

Where F_F, F_R is the tractive force for the front and rear axle, F_D is the air resistance and U is the velocity of the vehicle. The resistances due to rolling and slope are neglected (Belhocine and Wan Omar, 2018).But

$$F_F + F_R + F_D = ma, \text{ so } P_{tot} = maU$$

Let ϕ be the coefficient that represents the proportion of the braking force relative to the rear wheels; F_R = ϕmaU and F_F = (1-ϕ)maU

If *a* is constant, we have:

$$u(t) = U_0 - at \quad (2)$$

Also, the braking power delivered to the front brake disc is equal to half the total power for the front axle:

$$P_{totf} = \frac{(1-\varphi)}{2} ma(U_0 - at) \quad (3)$$

At t=0, we have

$$P_{totf} = \frac{(1-\varphi)}{2} maU_0 \quad (4)$$

We factor the braking efficiency Z which is the ratio between the deceleration of the vehicle (a) and the acceleration of gravity (g):

$$Z = \frac{a}{g} \quad (5)$$

$$P_{totf} = \frac{(1-\varphi)}{2} mZgU_0 \qquad [W] \quad (6)$$

Considering that the brake disc will absorb all the amount of heat generated during the braking phase (M. K. Khalid, M. R. Mansor, S. I. Abdul Kudus, M. M. Tahir, 2011), usually more than 90% is absorbed (Cruceanu, 2007), equation (1) shows the total heat flux entering the disc in Watts. We can also express it per surface area and in our case the surface area is the disc surface swept by the two opposing brake pads (A_S):

$$P'_{totf} = \frac{(1-\varphi)}{2} \frac{1}{2A_S} mZgU_0 \qquad \left[\frac{W}{m^2}\right] \quad (7)$$

Considering the factor of exploitation of the friction surface:

$$\varepsilon_p = \frac{P'_{totf}}{P'_{totfmax}} \quad (8)$$

We get the final form of the initial thermal flow of friction entering the disc:

$$q_0 = \frac{(1-\varphi)}{2} \frac{1}{2A_S\varepsilon_p} mgZU_0 \qquad \left[\frac{W}{m^2}\right] \quad (9)$$

1.4 Computational Fluid Mechanics

Computational Fluid Dynamics (CFD) is a branch of fluid mechanics that uses numerical analysis to solve problems involving fluid flows. High performance computers are used for the required calculations of the governing equations. With the rapid advance in computer capacity and speed, the CFD technique has become a powerful alternative for predicting airflows. In recent years, we have

seen major development in this area including the accuracy and speed of this method to predict the flow of a fluid in a wide range of engineering applications.

CFD analysis started in the 1960s with the solution of linear equations (Vincenti *et al.*, 1956), the 1970s with nonlinear inviscid flow simulation, the 1980s with the compressible Reynolds averaged Navier-Stokes equations and three-dimensional steady flow simulation, and the 1990s as the era for unsteady flow simulation (Deardorff, 1970; Huang, Bradshaw and Coakley, 1992; Maccormack, 1993). CFD analysis was mainly used for aerospace and military applications, but in the mid-1980s and 1990s, we saw automotive applications from manufacturers and teams in motorsport. These applications included external aerodynamics, air intake and heat transfer analysis. One example of CFD analysis in automotive vehicles is the work of (Kataoka *et al.*, 1991). Kataoka and his colleagues studied the contribution of active aerodynamic devices on the MlTSUBlSHl HSR II and the 3000GT. He also studied the effects on the maneuverability, which is improved by movable aerodynamic control devices and compared the results with the wind tunnel test results.

1.4.1 Governing equations

CFD is a group of computational methodologies, used to solve equations governing fluid flow. These equations are:

The continuity equation, which states that the rate at which mass enters a system is equal to the rate at which mass leaves the system plus the accumulation of mass within the system. The differential form of the continuity equation is:

$$\frac{\partial \rho}{\partial t} + \nabla * (\rho \boldsymbol{V}) = 0 \quad (10)$$

Where:

ρ is fluid density,

t is time,

$\boldsymbol{V} = ui + vj + zk$ is the flow velocity vector field.

The conservation of linear momentum which states that in a closed system the total momentum is constant and is implied by Newton's laws of motion. The differential form of this equation is:

$$x - component \qquad \frac{\partial (\rho u)}{\partial t} + \nabla * (\rho u \boldsymbol{V}) = -\frac{\partial p}{\partial x} + \rho f_x + (F_x)_{viscous} \quad (11)$$

$$y - component \qquad \frac{\partial(\rho v)}{\partial t} + \nabla * (\rho v \boldsymbol{V}) = -\frac{\partial p}{\partial y} + \rho f_y + (F_y)_{viscous} \quad (12)$$

$$z - component \qquad \frac{\partial(\rho z)}{\partial t} + \nabla * (\rho z \boldsymbol{V}) = -\frac{\partial p}{\partial z} + \rho f_z + (F_z)_{viscous} \quad (13)$$

Where:

ρ is fluid density,

t is time,

$\boldsymbol{V} = ui + vj + zk$ is the flow velocity vector field,

f is the net body force per unit mass exerted on the fluid,

$(F)_{viscous}$ is the viscous shear stresses.

For an incompressible flow, where ρ is constant, the primary flow-field variables are p and **V**. The continuity and momentum equations are two equations in terms of the two unknowns p and **V**. Hence, for a study of incompressible flow, the continuity and momentum equations are sufficient tools to do the job. However, for a compressible flow, ρ is an additional variable, and therefore we need an additional fundamental equation to complete the system. This fundamental relation is the energy equation:

$$\frac{\partial}{\partial t}\left[\rho\left(e + \frac{V^2}{2}\right)\right] + \nabla * \left[\rho\left(e + \frac{V^2}{2}\right)\right]\boldsymbol{V} = \rho\dot{q} - \nabla * (p\boldsymbol{V}) + \rho(\boldsymbol{f} * \boldsymbol{V}) + \dot{Q}'_{viscous} + \dot{W}'_{viscous} \quad (14)$$

Where:

ρ is fluid density,

t is time,

e is the internal energy per unit mass,

V is the local fluid velocity,

$\dot{q}$ is the volumetric rate of heat addition per unit mass,

$\boldsymbol{V} = ui + vj + zk$ is the flow velocity vector field,

f is the net body force per unit mass exerted on the fluid,

$\dot{Q}'_{viscous}$ is the rate of heat addition to the control volume due to viscous effects,

$\dot{W}'_{viscous}$ is the rate of work performed on the control volume due to viscous effects.

1.4.2 The Navier-Stokes equations

The Navier-Stokes equations are a set of coupled partial differential equations used to describe in a given flow, how the velocity, pressure, temperature, and density are related. They took their name from the Frenchman M. Navier and the Englishman G. Stokes, who independently obtained the equations in the first half of the nineteenth century. The Navier-Stokes equations consist of; a time-dependent continuity equation for conservation of mass, three time-dependent conservation of momentum equations and a time-dependent conservation of energy equation. There are four independent variables, the x, y, and z spatial coordinates of a domain, and the time t. Also, there are six dependent variables; the pressure p, density ρ, temperature T and velocity vector **V**. The complete Navier-Stokes equations with the body forces being neglected (Anderson, 2011) and the viscous terms expressed explicitly are shown below:

$$\frac{\partial \rho}{\partial t} + \nabla * (\rho \boldsymbol{V}) = 0$$

$$x - component \qquad \rho \frac{Du}{Dt} = -\frac{\partial p}{\partial x} + \frac{\partial \tau_{xx}}{\partial x} + \frac{\partial \tau_{yx}}{\partial y} + \frac{\partial \tau_{zx}}{\partial z}$$

$$y - component \qquad \rho \frac{Dv}{Dt} = -\frac{\partial p}{\partial y} + \frac{\partial \tau_{xy}}{\partial x} + \frac{\partial \tau_{yy}}{\partial y} + \frac{\partial \tau_{zy}}{\partial z}$$

$$z - component \qquad \rho \frac{Dw}{Dt} = -\frac{\partial p}{\partial z} + \frac{\partial \tau_{xz}}{\partial x} + \frac{\partial \tau_{yz}}{\partial y} + \frac{\partial \tau_{zz}}{\partial z}$$

$$\rho \frac{D(e + V^2/2)}{Dt} = \rho \dot{q} + \frac{\partial}{\partial x}\left(k \frac{\partial T}{\partial x}\right) + \frac{\partial}{\partial y}\left(k \frac{\partial T}{\partial y}\right) + \frac{\partial}{\partial z}\left(k \frac{\partial T}{\partial z}\right) - \nabla * p\boldsymbol{V} + \frac{\partial (u\tau_{xx})}{\partial x} + \frac{\partial (u\tau_{yx})}{\partial y} + \frac{\partial (u\tau_{zx})}{\partial z} + \frac{\partial (u\tau_{xy})}{\partial x} + \frac{\partial (u\tau_{yy})}{\partial y} + \frac{\partial (u\tau_{zy})}{\partial z} + \frac{\partial (u\tau_{xz})}{\partial x} + \frac{\partial (u\tau_{yz})}{\partial y} + \frac{\partial (u\tau_{zz})}{\partial z}$$

Note that the normal and shear stresses that appear can be expressed in terms of the velocity field, but such substitution would occupy too much space. These viscous flow equations are nonlinear and do not have any general analytic solutions. There are various ways to approach the solution for these equations. One way is to apply them to a problem which by nature, will allow some terms of the equations to be zero and the resulting system of equations will be a lot simpler to be solved, either

with an analytical solution or a simple numerical one. An example are the boundary-layer equations discussed in section 1.5. Another way is to make some approximations and neglect certain terms that have a very small value in a given problem. The simpler, but still nonlinear boundary-layer equations are a classic example of that approach. Finally, a very promising approach is to apply numerical methods to solve the full viscous flow equations using CFD.

1.4.3 CFD approaches to turbulence modeling

In computational modeling of turbulent flows, one must consider the computational cost of the modeling process. The range of scales that are modeled and the intricacy of the phenomena will determine the cost. Turbulence is a phenomenon characterized by a chaotic change in pressure and velocity of the flow and is the main obstacle to many practical applications of CFD (McComb, 1990). There are three general approaches to turbulence: direct numerical simulation (DNS), large-eddy simulation (LES), and Reynolds-averaged Navier-Stokes (RANS) equation simulation with turbulence models.

1.4.3.1 Direct Numerical Simulation (DNS)

The direct numerical simulation of turbulence is the most straightforward approach as it directly solves the Navier-Stokes equations without any approximations. In principle, all the scales of motion in a fluid flow can be resolved accurately (Shang, 2004) and DNS resolves the whole range of spatial and temporal scales of the turbulence, from the smallest dissipative scales (Kolmogorov scales) to the integral scale, which is associated with the motions containing most of the kinetic energy (Zhang *et al.*, 2007). According to the Kolmogorov microscales, the ratio between the largest and smallest eddy of fluid motion is proportional to the three-quarter power of the characteristic Reynolds number, $Re^{3/4}$ (Björgum, 1961). For this reason, a very fine discretization technique should be used as the number of grid points required to describe turbulent motions should be proportional to $Re^{9/4}$ (Nieuwstadt *et al.*, 1994). This method, although accurate, has extremely high computational costs and will not be considered for this study.

1.4.3.2 Large Eddy Simulation (LES)

Large Eddy Simulation was developed in the 60s and is based on the hypothesis that turbulent motion can be divided into large and small eddies (Smagorinsky, 1963; Deardorff, 1970). According to (Kolmogorov, 1941), large eddies are responsible for the majority of the kinetic energy of the flow and are a characteristic of the geometry of the model, where small eddies are more universal, and it is easier to model them without compromising the accuracy of the model. Furthermore, large eddies are responsible for most of the transport phenomena occurring in the flow. With this in mind, large eddies are directly linked with the viscous flow equations and are being simulated without any

modeling, whereas for small eddies an approximation is used. LES puts a high demand on a computer requiring a fine grid and small-time step but will produce accurate results and with the development in computing power, this method seems to gain more ground in CFD analysis.

1.4.3.3 Reynolds Averaged Navier-Stokes equations (RANS)

The RANS equations are time-averaged NS equations using Reynolds's decomposition. Reynolds decomposition is a mathematical technique where the value of a certain variable (i.e. velocity) could be written as the sum of the time-averaged value plus the fluctuations of that variable (Reynolds, 1895). Since the NS equations are non-linear, a non-linear acceleration term appears when averaging the NS equations. This term is known as Reynolds Stress $= \rho\overline{u_\iota{}' u_j{}'}$ and cannot be solved directly, but instead is modeled using a turbulence model. This approach is the most common as it provides sufficient results with very low computational costs. RANS turbulence models are divided into two primary categories: eddy-viscosity models and Reynolds-stress models. Eddy-viscosity models are classified according to the number of extra transport equations used to "close" the RANS equations. We will concentrate in the two equations models and more specifically in the k-ε and k-ω models.

The standard k-ε model is used to close RANS by introducing transport equations for the turbulent kinetic energy, k, and dissipation rate of k, ε, to obtain the eddy viscosity. By solving two partial differential transport equations, we are able to incorporate more turbulence physics into the model. The turbulent eddy-viscosity is calculated as:

$$\nu_T = C_\nu \frac{k^2}{\varepsilon} \quad (15)$$

Where C_ν is an empirical constant equal to 0.09.

Then the eddy-viscosity can be applied to the Boussinesq approximation to relate the turbulence stresses to the mean flow.

Boussinesq approximation:

$$-\overline{u_\iota{}' u_j{}'} = \nu_T \left(\frac{\partial \overline{u}_\iota}{\partial x_j} + \frac{\partial \overline{u}_j}{\partial x_i} \right) - \frac{2}{3} \mathrm{k} \delta_{ij} \quad (16)$$

Where:

ν_T is the turbulence eddy viscosity,

$\mathrm{k} = \frac{1}{2}\overline{u_\iota{}' u_\iota{}'}$ is the turbulent kinetic energy,

and δ_{ij} is the Kronecker delta.

The standard k-ε model is the most common model, used for its robustness and low computing costs but may struggle in near-wall conditions, or for flows with high pressure gradients. For this reason, the realizable k-ε model was developed. The realizable k-ε model differs from the standard in two ways. Firstly, in the equation for the eddy-viscosity the C_ν becomes a variable. Secondly, a slightly different transport equation for the dissipation rate ε is used. These changes provide the normal stresses to be positive, making the model realizable. This model will produce better results in capturing the mean flow for more complex designs and rotational flows.

The k-ω model is a two-equation eddy-viscosity model used to close RANS, where ω is the specific dissipation and is defined as:

$$\omega = \frac{\varepsilon}{k} \quad (17)$$

According to (Wilcox, 1988; Menter, 1992) the k-ω model will provide better results in near -wall conditions and in flows with high pressure gradients, but will struggle, compared to the k-ε model, in the wake regions of the flow (Menter, 1992). Research has shown that the k-ω model cannot be applied for unambiguously for industrial types of applications (Menter, 1992). This led to the development of a new model that combines the best characteristics of the two models, called shear stress transport (SST) k-ω model developed by Menter in 1994. To achieve this, the standard high-Reynolds-number version of the *k-ε* model will be multiplied by a blending function $(1 - F_1)$. The blending function will be designed to be one in the inner layer (viscous sublayer and logarithmic region) of the boundary layer and to gradually switch to zero in the wake region (Menter, 1994a). This method requires more computation but has better overall performance.

1.5 Boundary-layer theory

A boundary-layer is a thin region of flow adjacent to a solid surface were certain parameters of the flow, such as velocity and temperature, appear different from their free-stream values, due to the friction between the fluid and surface.

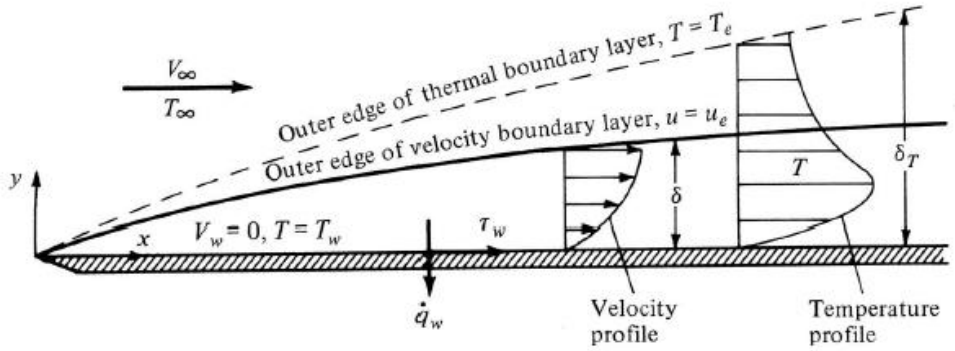

Figure 8 Boundary-layer over a flat plate

As shown above (Anderson, 2011), certain properties of the boundary-layer can be seen, such as the velocity and temperature profile, the velocity boundary-layer thickness δ and the thermal boundary-layer thickness δ_T. The influence of friction between the flat plate and the fluid adjacent to the flat plate (wall) acts to create a frictional force which retards the relative motion. This tangential force per unit area is defined as the shear wall stress τ_w. This causes the retardation of the fluid and at the wall the fluid velocity equals to zero, $V_w = 0$. This is called the no-slip condition. Likewise, the fluid temperature at the wall equals the temperature of the wall, $T = T_w$. Above the body surface, the fluid velocity increases in the y direction, until it reaches the free-stream value. The cause of the velocity and temperature gradient at the wall is the generation of shear stress and heat transfer respectively. Another property of a boundary-layer is the displacement thickness δ^*.

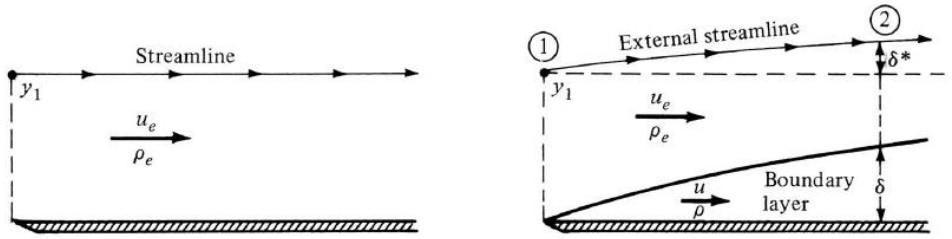

Figure 9 Hypothetical inviscid flow over a flat plate (left) and viscous flow with a boundary-layer (right)

As shown in the previous figure (Anderson, 2011), the displacement thickness represents the deflection of the streamline external of the boundary-layer by δ^*, as the boundary-layer is seen as an obstruction from the free-stream flow. Since the free-stream flow is deflected, the shape of the actual body "visible" by the free-stream is the physical body plus the deflection and is called the effective body. Boundary-layers are a very important concept in the field of aerodynamics as it provides practical solutions for calculating aerodynamic drag and flow separation. Because of the properties of boundary-layers, we are able to derive the boundary-layer equations, which are a simpler version of the Navier-Stokes equations applicable inside the boundary-layer. The boundary-layer equations may be nonlinear partial differential equations, like the NS, but they are much simpler, and we are able to obtain analytical solutions.

Boundary-layers can be divided into *laminar boundary-layers* and *turbulent boundary-layers*. In almost every physical problem there is turbulence present and so the study of turbulent boundary-layers is essential for the kind of problems this thesis will deal with. Unfortunately, turbulence is still an unsolved problem in fluid mechanics, and we do not have a complete understanding of this phenomenon. All solutions regarding turbulent boundary-layers are some sort of an approximation using turbulence models, such those discussed in section 1.4. Within a boundary layer, we can distinguish different regions with different characteristics. Those regions are defined by y^+. y^+ is a dimensionless number which represents the distance from the wall in terms of viscous lengths. As explained by (Cengel and Cimbala, 2017), a boundary layer consists of 4 regions. First, the viscous sublayer which is the one closest to the wall surface. Viscous effects around this area are very dominant and the flow is streamlined and the velocity profile nearly linear. Next up is the buffer sublayer. Turbulence is starting to take effect but, the flow is still dominated by viscous effects. In the overlap layer turbulent effects are getting bigger and finally in the turbulent layer, turbulence is the most dominant in the flow.

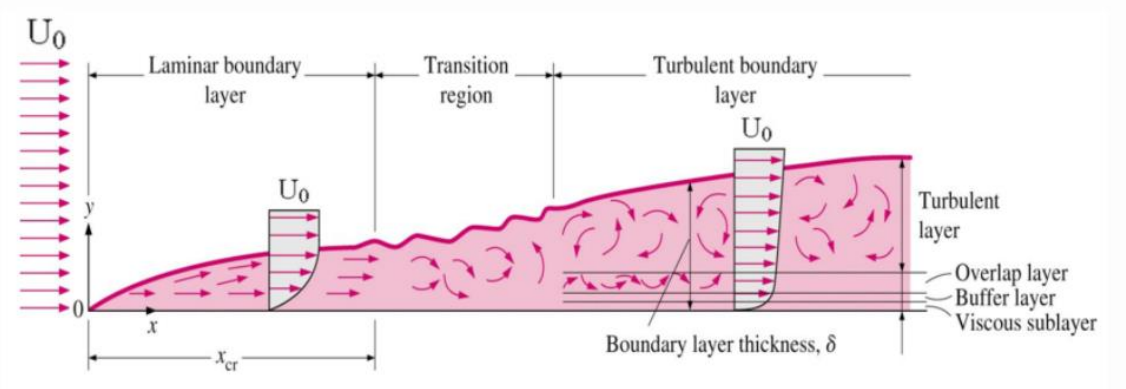

Figure 10 The development of the boundary layer for flow over a flat plate, and the different flow regimes

2. Methods

2.1 Design

At the start of the designing process, we must take into consideration the topology of the vehicle that will be fitted with the brake duct. In high performance road cars and touring car racing, the wheels of the vehicles are closed, and a need of a long duct is necessary to direct the air to the discs. By utilizing openings in the front bumper of the vehicle, we essentially design the inlet of the duct. Then, a long flexible tube is used to direct the air around all the different compartments of the car and finally to the outlet. In this thesis, we will be focusing on open wheel racing, like Formula 1 racing, where most of the suspension components and the wheels of the vehicle are completely open and exposed to the ambient air stream.

Several design ideas where considered. First, a duct with a circular cross section was designed as shown in the figure below.

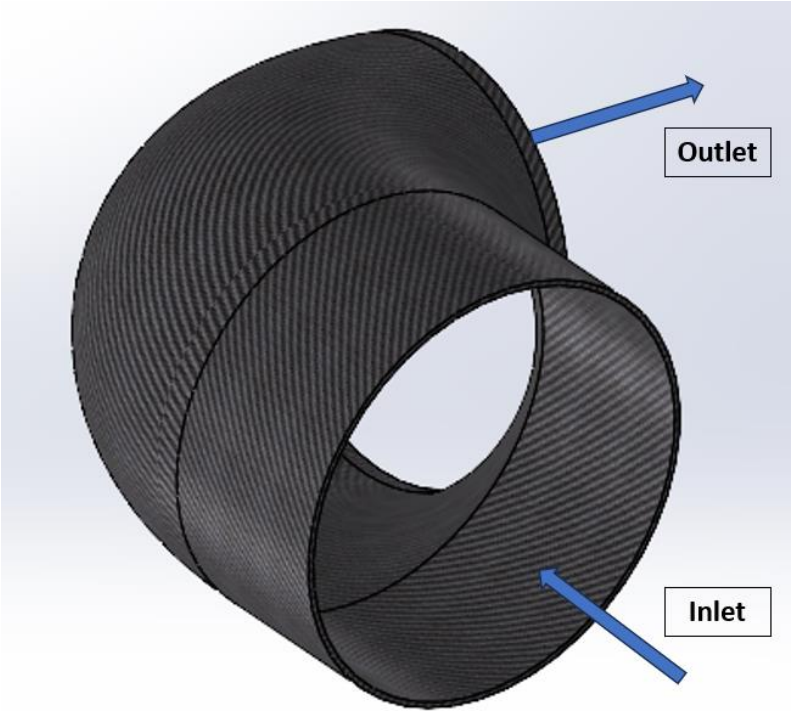

Figure 11 Duct with a circular cross section

The benefits of such a design are the fact that it is very easy and cheap to produce and, aerodynamically speaking, very efficient. But, to achieve a substantial surface area, we would need a lot of space, especially along the axis parallel to the ground. That is where most of the suspension components are, like the track rods, wishbones, push and pull rods. In order, to create a duct that is using more space in the axis perpendicular to the ground, a second design was created, with an oval cross section.

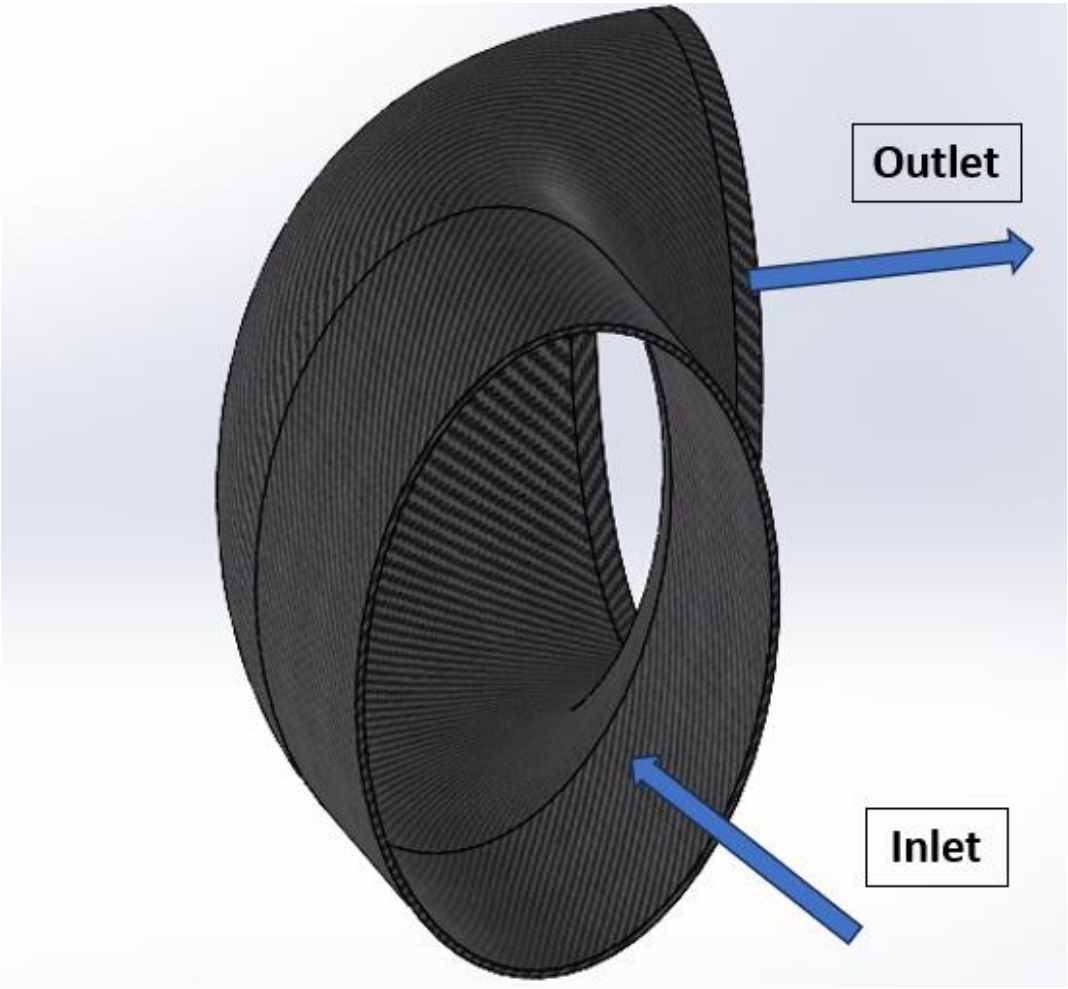

Figure 12 Duct with an oval cross section

Having to use an oval duct, we can keep the benefits of the circle (i.e., simple design and low drag) but we are now using less space in the already “busy” region of the suspension elements. Next, a need to split the airflow inside the duct was created, thus enabling us to direct the cool air to different regions of the brake assembly. Having an oval cross section would result in a very complicated design, raising the cost of production. So, we designed a new cross section which, essentially, is a parallelogram with rounded corners. This design will provide us with a very good starting point to create the two different outlets for the airflow and still be an aerodynamically and topologically acceptable air duct.

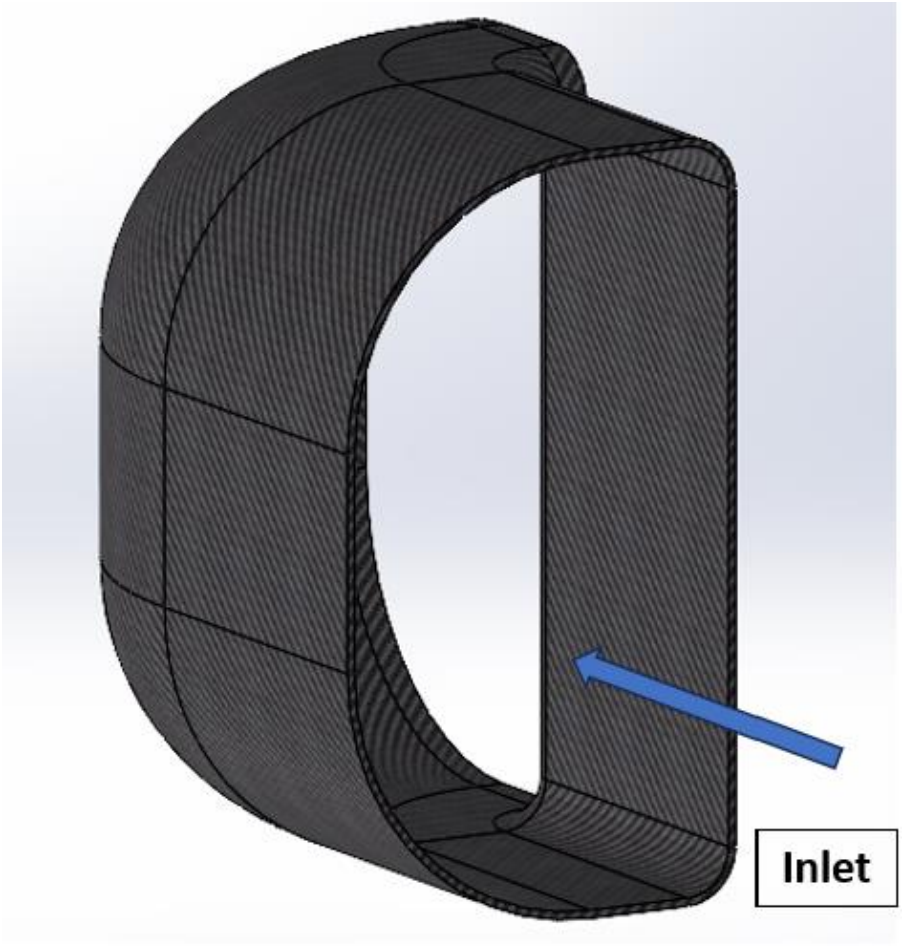

Figure 13 Duct with the final cross section

A brake duct with a parallelogram with rounded corners cross section offers significant advantages specifically tailored for race cars. Its unique cross-sectional shape plays a crucial role in optimizing aerodynamic performance on the racetrack. By reducing drag and minimizing turbulence, the duct enables race cars to achieve higher speeds and better overall lap times. The efficient airflow management provided by this design directs a continuous stream of cooling air towards the brakes, effectively dissipating heat generated during intense braking maneuvers. The rounded corners of the parallelogram shape further enhance the duct's aerodynamic efficiency by reducing air resistance contributing to improved vehicle stability at high speeds.

After carefully taking into consideration all the bibliography (Jeong *et al.*, 2014b; Luiz Filipe de Medeiros Gomes *et al.*, 2018) and the needs of a racing car when it comes to performance and costs, the final design of the brake duct must incorporate the aerodynamic design for the lowest possible drag, but at the same time it needs to separate the flow in two different ones. The cross section should be close to a circle and that is clearly shown in the Figure below with the duct next to the brake disc.

Figure 14 Final assembly

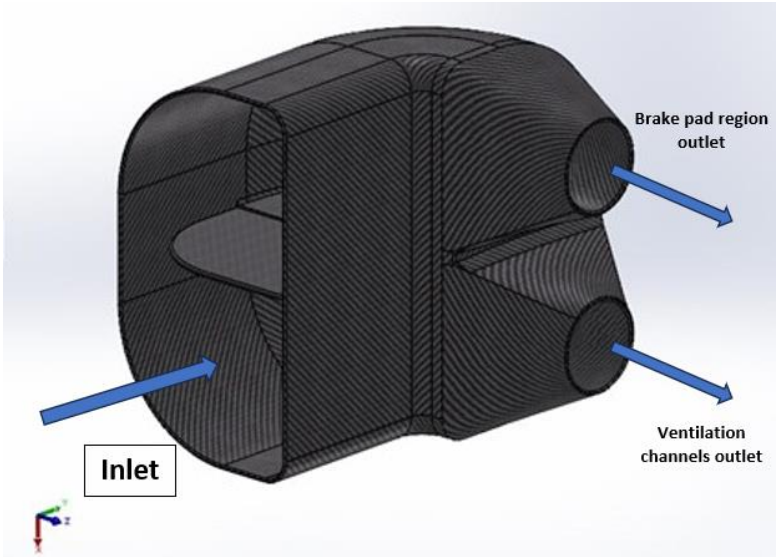

Figure 15 Brake duct assembly

By splitting the air supply with the use of a moving flap we can create two different air channels, each with its own purpose. The top channel will direct air through a convergent nozzle shaped outlet to the brake pad region. The bottom channel will supply with cool atmospheric air the ventilation channels of the brake disc.

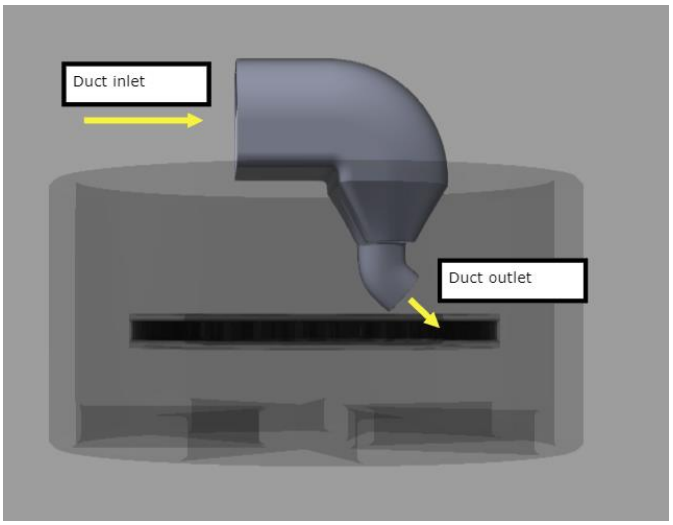

Figure 16 Angled duct outlet providing cool air to a specific part of the brake region.

During a race or during a single lap, the cooling needs of the brake region can vary significantly. After heavy braking, the brake discs can reach extremely high temperatures and if by the next corner they are not cool enough, the driver will experience brake fading, resulting in a loss of performance. Also, after a long straight, the brake discs might have cooled too much experiencing temperatures lower than the ideal ones resulting in the driver not maximizing the car's braking capabilities. A great way to monitor the cooling of the brake disc and the brake pad region, which cannot exceed a certain temperature, is an active brake duct which will always supply the different brake regions with the correct amount of air. The flap is designed to rotate from 0° (horizontal position) to ±25° increasing or decreasing the inlet surface area of the top and bottom channels as shown in the following figures.

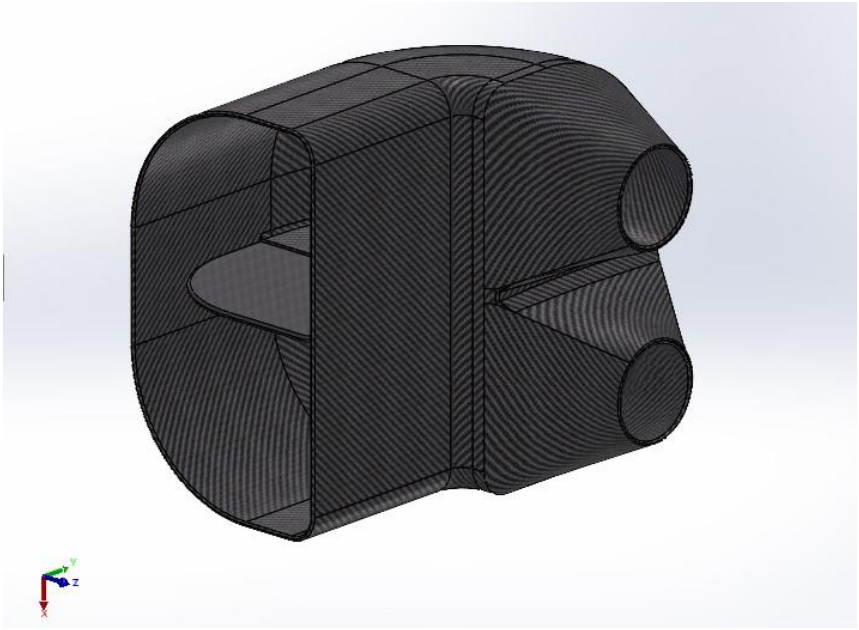

Figure 17 Duct with the flap at 0° angle (horizontal)

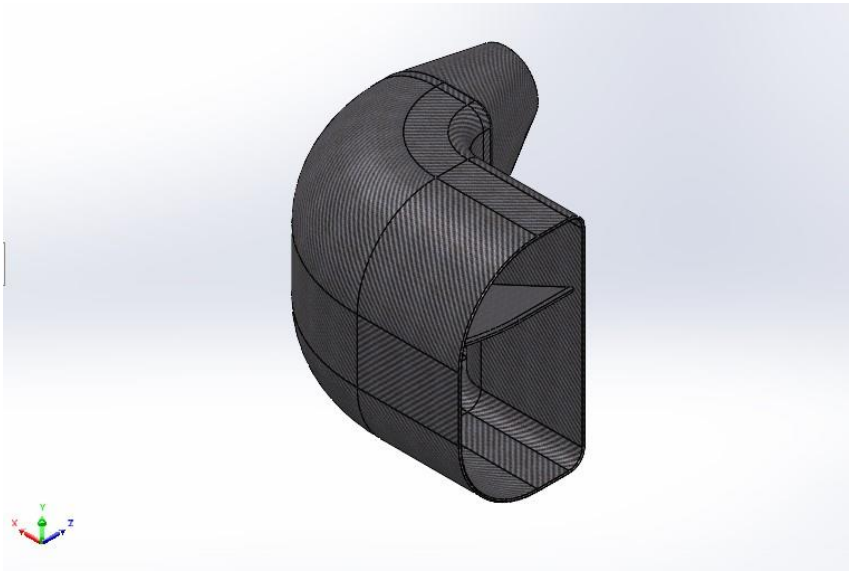

Figure 18 Duct with flap at 25° angle

The calculated surface area of the whole inlet is 95 cm^2 and with a flap angle of 25° the air is distributed 70% to the disc ventilation channels and 30% to the brake pad area and vice versa.

The following figure shows a brake duct assembly of the W11 Mercedes Formula 1 team race car. The blue arrow on the right shows the duct inlet and we can immediately see that there are 5 different airflow channels. The whole duct assembly is coupled to the car via the suspension arms.

Since we will be focusing only on the aerodynamic characteristics of the duct, the suspension parts will not be included in the analysis.

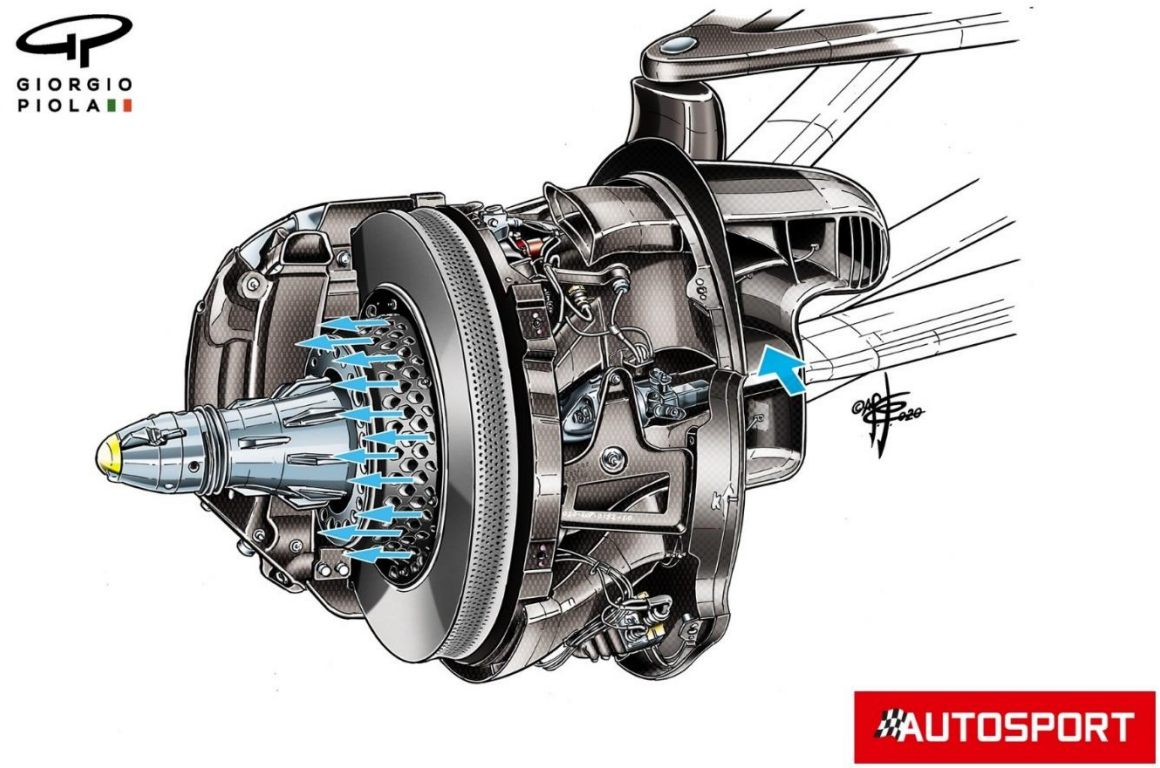

Figure 19 Mercedes W11 brakes and cooling duct. Autosport.com, 2021, accessed on 5/5/2023, https://www.autosport.com/f1/news/how-mercedes-and-red-bull-have-diverged-on-f1-brake-duct-ideas/6741111/.

2.2 Meshing and fluid regions

For the calculation of the computational model a surface and volume mesh need to be created and for this reason I used ANSYS Fluent. ANSYS Fluent is a fluid simulation program that contains all the physical modelling capabilities needed for the simulation of fluid flow, turbulence, heat transfer and more. Since our simulation includes a rotating fluid region i.e., the brake disc ventilation channels and the wheel, we need to set up the simulation using a Multiple Reference Frame (MRF) mesh environment. In computational fluid dynamics (CFD), the concept of multiple reference frames (MRF) is used to simulate flow problems involving rotating or moving components within a fixed computational domain. It is a technique that allows the modeling of flows in systems where different parts of the domain are in relative motion with respect to each other. The MRF approach is particularly useful when dealing with problems such as rotating machinery, turbomachinery, or vehicles with

moving parts. Instead of simulating the entire domain with a single reference frame, the computational domain is divided into multiple regions or zones, each associated with its own reference frame. These reference frames can be stationary or moving at different speeds and directions. Each reference frame is defined by a coordinate system attached to the moving or rotating component. The equations governing fluid flow, such as the Navier-Stokes equations, are solved separately in each reference frame. The flow variables (e.g., velocity, pressure, temperature) are typically transformed between different reference frames using appropriate coordinate transformations. The MRF approach simplifies the simulation by decoupling the relative motion of different parts of the domain and treating them independently within their respective reference frames. This reduces the computational complexity and allows efficient modeling of problems involving complex geometries and moving components. It also helps to capture the physics associated with the relative motion of different regions accurately. To ensure consistency and continuity between different reference frames, appropriate interface conditions or boundary conditions are applied at the interfaces between the zones. These conditions define how information is exchanged or transmitted between the different reference frames. For example, the velocity and pressure may be matched or interpolated at the interfaces to maintain continuity across the boundaries. In summary, the multiple reference frame technique in CFD enables the simulation of flow problems involving relative motion between different regions of the computational domain. It provides an efficient and accurate approach to model complex systems with rotating or moving components, such as turbines, propellers, or vehicles with rotating wheels. The areas of our control volume that require special treatment i.e., a fine surface and volume mesh, are the inlet and outlet of the duct, the brake pad region, and the ventilation channels. The fluid domain will be a rectangular shaped wind tunnel with the following measurements:

Table 1 Fluid domain

Fluid domain (meters)	
Length	3.0
Width	1.2
Height	1.3

The domain must be big enough to calculate the results without the interference of the walls. Since our main goals are the control of wind velocity in the ventilation channels and the brake pad region, with the utilization of the duct flap, the wheel assembly will be placed high enough from the “ground” so it’s effects will be negligible.

First, a surface mesh is being created while giving extra care for the ventilation channels and brake pad region. As stated in relevant literature (Yadav and Lanfrit, 2005) for external vehicle aerodynamics the mesh should meet certain requirements. First, the creation of the surface mesh will be implemented, consisting of triangular elements, the most common element type in CFD. For external aerodynamics, being able to calculate the pressure variations to derive the Drag and Lift coefficients is very important. Pressure variations occur in many areas in our design; inside the duct, inside the brake disc channels, in the wake of the duct etc. Most of the areas where we must create a very fine mesh, are geometries with a large amount of curvature, creating flow separation and reattachment. A fine surface mesh will also provide a solid foundation for the creation of the volume mesh. The criteria which will be used for the validation of the surface mesh are skewness, surface wrapping and min/max angle.

Skewness is defined as the variation of an element from the “ideal” and in our case, an equilateral triangle. According to ANSYS documentation a value of 0 results in the best possible element and a value of 1 as the worst possible scenario. A value larger than 1 is not permitted. The formula for the calculation of skewness is:

$$Skewness = \frac{(A_0 - A)}{A_0} \quad (18)$$

Where:

A_o is the surface area of an equilateral surface element (triangle).

A is the surface area of the generated element.

Surface wrapping is only applicable in quad elements where two triangles are created by a line along the diagonal. The angle between the two triangles is measured. According to ANSYS documentation the default maximum angle between the two planes specified is 40°.

Finally, the angle between two adjacent edges in a triangular element is measured. Again, the ideal would be an equilateral triangle, i.e. 60° max angle. In ANSYS there is a minimum angle limit at 30° to ensure a sufficient skewness value.

$$Angle = max\left(\frac{\max(\varphi_i) - A}{180 - A}, \frac{A - \min(\varphi_i)}{A}\right) \quad (19)$$

Where:

A is the ideal 60° angle

ϕ_i is the angle of the triangle with i = 1,2,3

a value of 0 represents a "perfect" equilateral element.

Next up is the creation of the boundary layers to resolve the boundary layer which will be created along the surface of each geometry. Using the Inflation algorithm from ANSYS, hexahedral elements will be extruded from the triangular surface mesh to accurately represent the boundary layer conditions. For this step to take place we must define the height of the first element and the growth rate of the elements above it. By taking into consideration the velocity and the characteristic length of each geometry, we are able to calculate the thickness of the boundary layer, thus the height of the first element and the growth rate. To calculate the thickness of a turbulent boundary layer, we can use an approximation by (Anderson, 2011):

$$\delta = \frac{0{,}37 * x}{Re^{0.2}} = \frac{0{,}37 * 0.28}{598.000^{0.2}} = 7mm \ (20)$$

Where:

δ is the boundary layer thickness

x is the characteristic length of the geometry studied

Re is the Reynolds number (defined by the length of the brake duct).

Finally, a volume mesh is generated using Tetrahedral (Tetra) elements. Tetra elements are 3D elements which have been extracted by 2D triangular elements. Since not all regions of the domain need the same element size, the elements closer to the wall surfaces will have a smaller size, compared with the elements "far away" from the wheel assembly. Using the ANSYS body of influence function, we can create a region in our domain with finer mesh, thus resolving at a better rate the various fluid phenomenon. More specifically, for the brake pad region, a sphere of influence was used to create a finer mesh. The fluid domain mesh shown in figure 20 consists of hexahedral elements that correspond to the volume of air inside this "computational" air tunnel with a rectangular cross section.

Figure 20 and 21 also show the Inlet of the fluid domain and can be easily depicted by the triangular surface elements in figure 20. The final mesh parameters are shown below:

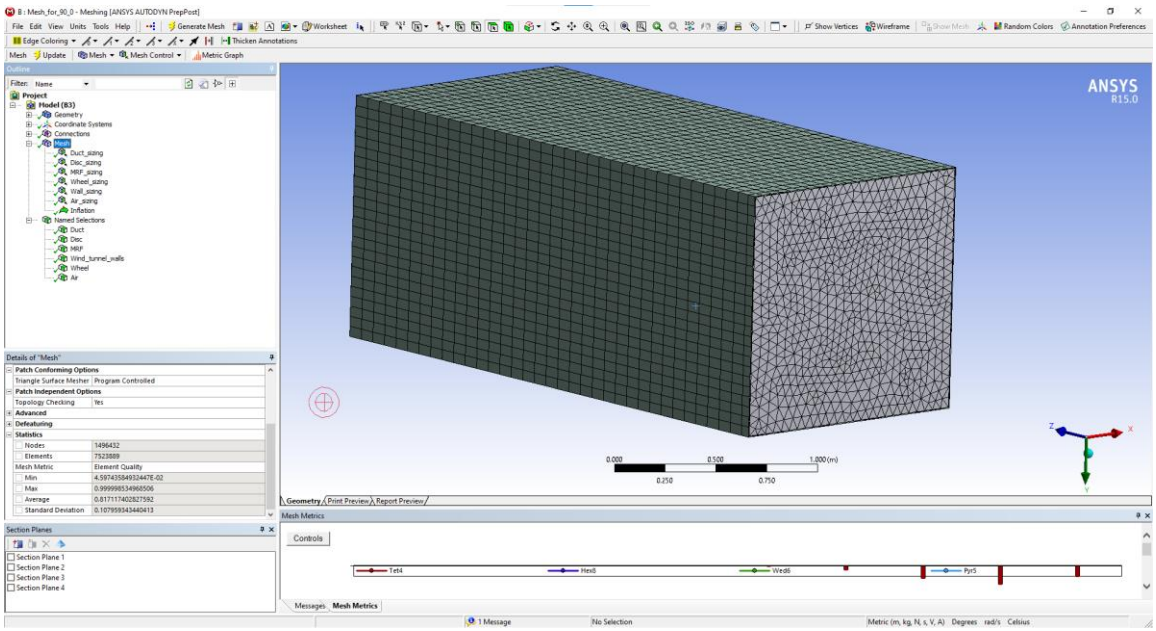

Figure 20 Domain with mesh

Nodes	≈1.5mil
Elements	≈6.5mil
# of layers	5
Growth rate	1.2

Table 2 Mesh parameters

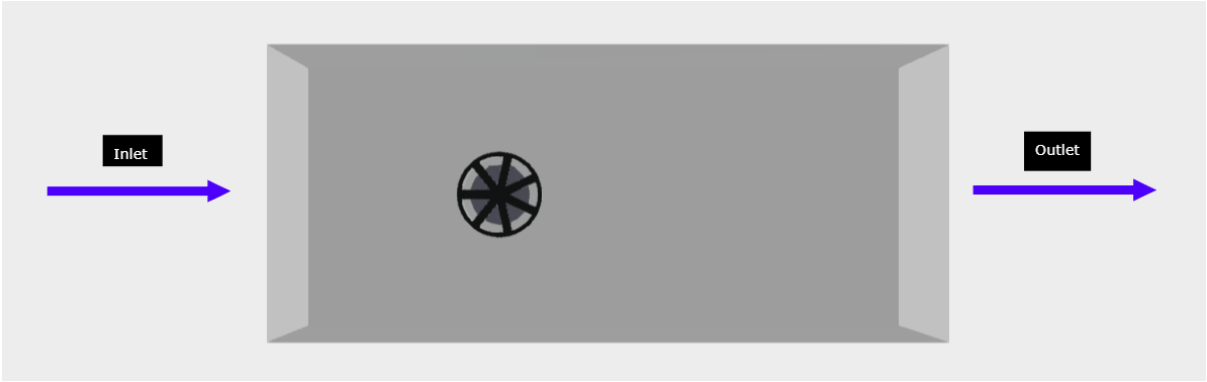

Figure 21 Computational domain with inlet and outlet.

Figure 22 displays a cross-section of the fluid domain perpendicular to the brake disc's rotation axis. The mesh elements in the image exhibit a coarser structure towards the domain's edges, represented by larger triangular elements. However, as we move closer to the assembly, the mesh becomes finer, indicating smaller and more densely distributed elements. In the figure, number 1 corresponds to the cross-section of the wheel, number 2 represents the duct's cross-section, and number 3 denotes the brake disc.

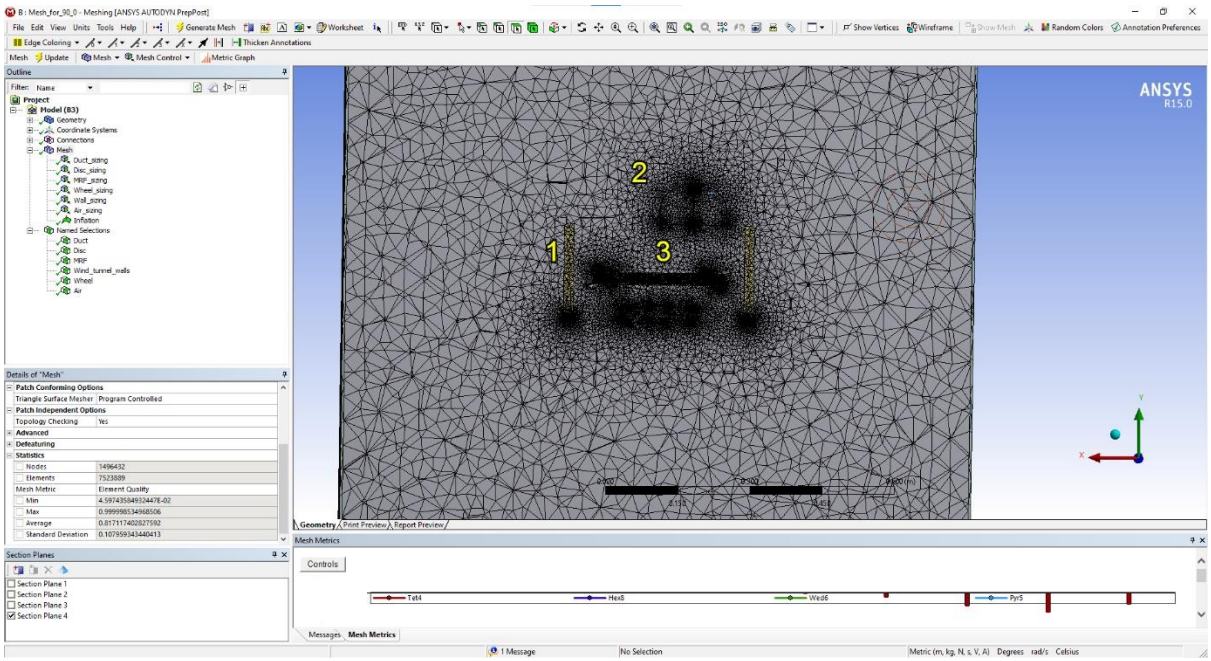

Figure 22 Cross section of the domain

2.3 Setting up the solver

For the Fluent solver the following parameters were set. For the viscous model, as mentioned in section 1.4.3.3, we are using the k-omega SST model that will provide better results in near wall regions (Menter, 1994b).

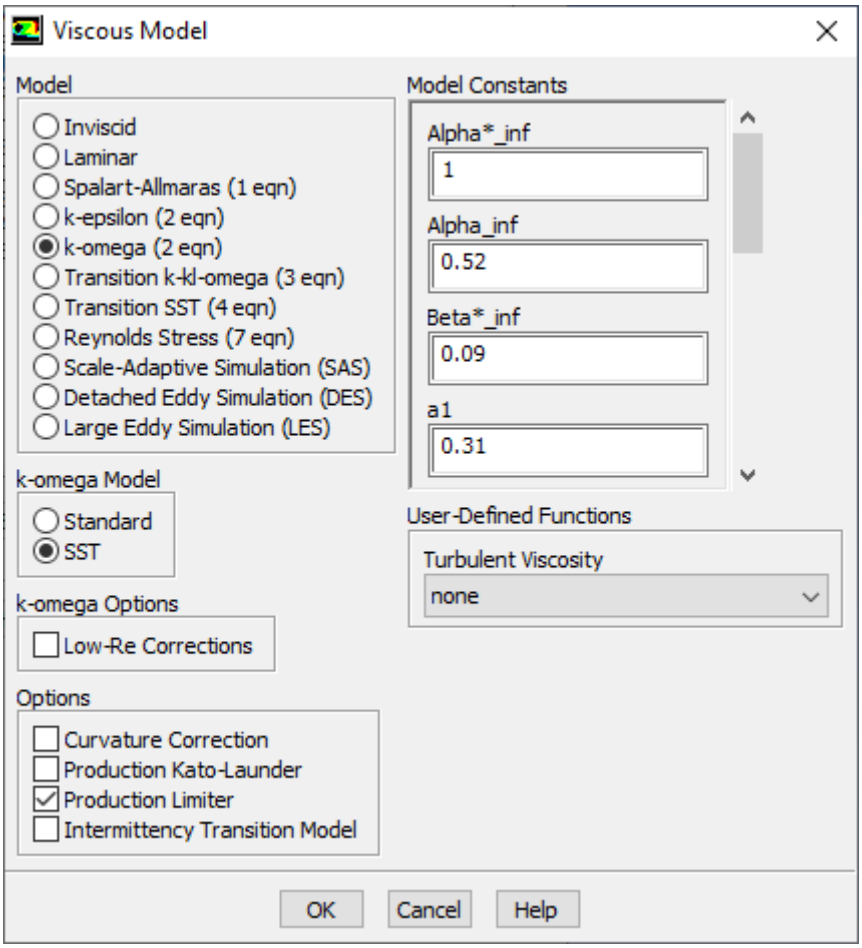

Figure 23 Viscous model

In the k-omega SST (Shear Stress Transport) turbulence model in ANSYS Fluent, the model constants alpha, beta, and a1 are parameters used to define the behavior of the model. These constants influence the turbulence modeling equations and determine the model's accuracy and performance. The values of these constants are typically set by the software developers and are not meant to be modified by the user.

Then, we specify the inlet conditions of the computational air tunnel, as shown in section 2.2 (Figure 21), and more specifically, the velocity magnitude.

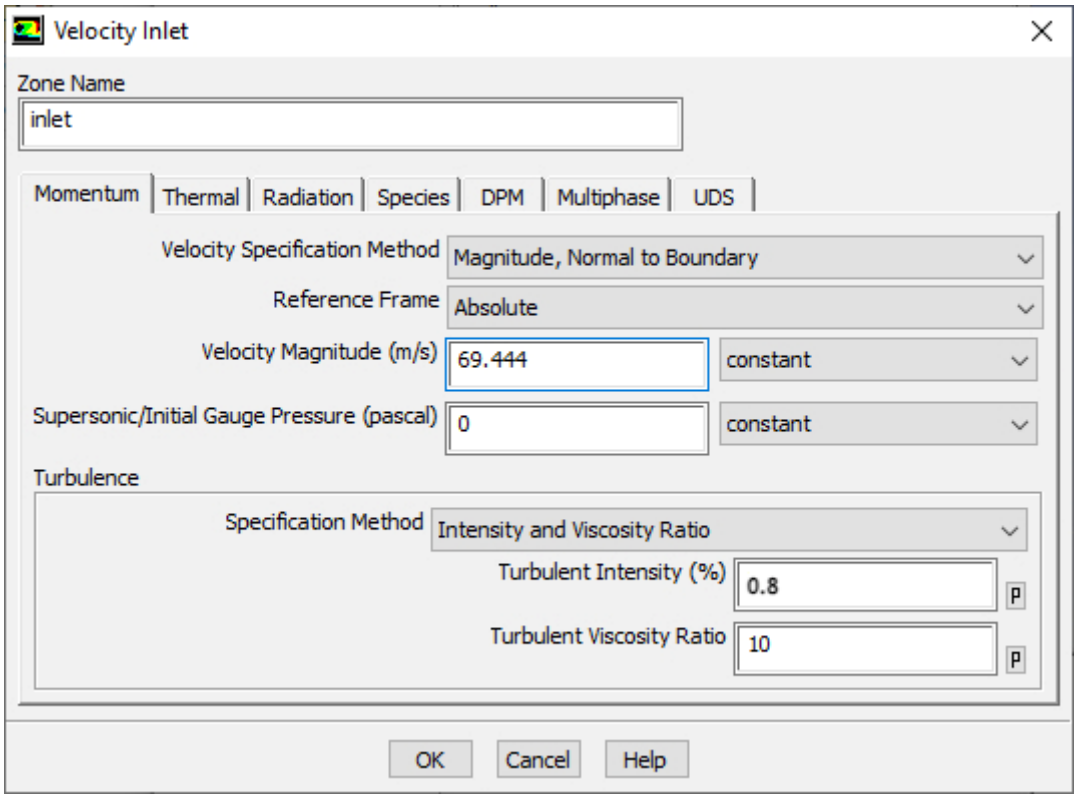

Figure 24 Inlet boundary conditions

According to the ANSYS documentation, the viscosity ratio is the ratio of the molecular viscosity of the fluid to the turbulent viscosity. It provides a measure of the relative influence of molecular viscosity compared to turbulent viscosity in the flow. Typically, the viscosity ratio is set between 1 and 10. For high Reynolds number, 10 is the desired choice. Turbulence intensity represents the magnitude of turbulence fluctuations within a flow. It quantifies the level of turbulence energy present in the flow field.

Calculating Reynolds number:

$$Re = \frac{\rho V L}{\mu}$$

Where:

ρ is the air density

V is the air velocity

L is the characteristic length of the duct

μ is the dynamic viscosity

The density of air can be taken as approximately 1.225 kg/m³.

The dynamic viscosity of air depends on temperature. Assuming a typical value of 20°C, the dynamic viscosity of air is approximately 1.7894 × 10^−5 kg/(m·s).

Now, we can calculate the Reynolds number:

$$Re = \frac{\rho V L}{\mu} = 598.000$$

To calculate the turbulence intensity:

$$I = 0.16 * Re^{(-1/8)} = 0.16 * 598.000^{(-1/8)} = 0{,}827\%$$

When it comes to the outlet conditions, we assume normal atmospheric conditions, thus ordering ANSYS to consider the outlet as a pressure outlet with a gauge pressure value of 0 Pa. The walls of the air tunnel and all other solid regions of the model are considered as stationary wall.

Finally, we set up the MRF zone. According to (Patil *et al.*, 2021) the fluid region that includes the ventilation channels needs to be modeled in a different reference frame in order to compute the rotational effect of an object, in our case the brake disc. We specify the material as “Air” and frame motion is selected. Then, we select the rotation axis and the rotational speed.

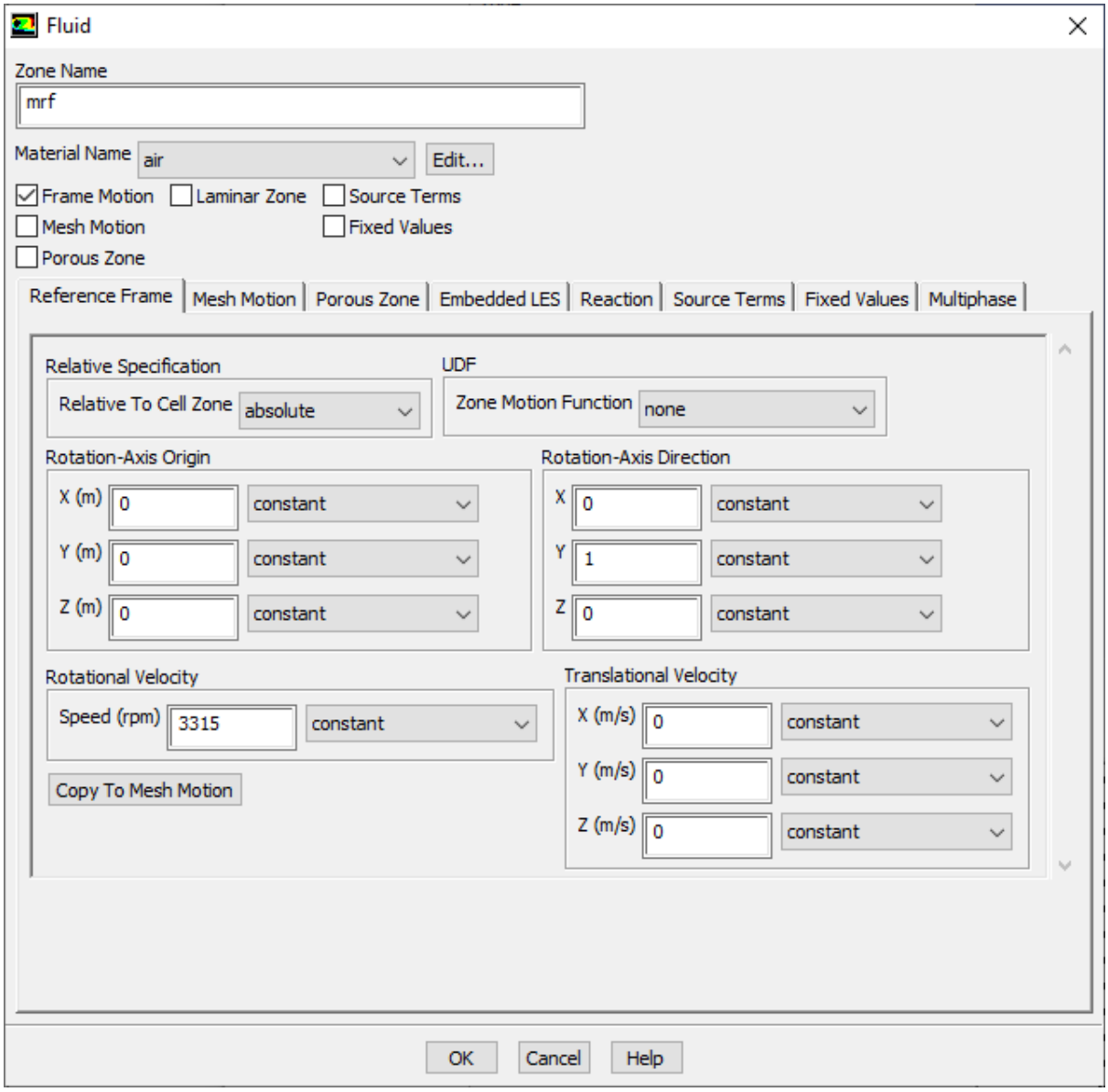

Figure 25 MRF zone

3. Results and Discussion

Using ANSYS Fluent's built in post-processing tools we can extract velocity contours on the different regions of interest. First, we obtain the results of the ductless simulation. This will be the baseline for all the coming simulations, as it is the best way to validate the performance of the brake duct. The rotational speed was set to 3315 rpm which corresponds to a vehicle velocity of approximately 250 Km/h or ≈69 m/s. The aim is to calculate four different parameters in order to be able to assess the importance of the duct. Those parameters are: Min velocity, Max velocity, Average velocity and Flow rate. The measurements were perfomed using ANSYS Fluent's function calculator. For the outlet velocities, we measured on a circular plane, 1cm from the duct exit (Hudson and Ruhl, 1997). For the vane velocities we measured on a circular plane, at the middle of the vane profile. Finally, the vanes inlet is considered the eye of the brake disc and the brake pad region is a circular plane located a few centimetres from the disc, where the brake pads and brake callipers will be located.

3.1 No duct case

In the absence of a brake duct, a careful examination of the figures reveals the airflow pattern and allows us to identify specific regions of the brake disc with varying velocities. By analyzing the figures, it becomes evident that the bottom region of the brake disc experiences a higher velocity airflow. This phenomenon is primarily influenced by the direction in which the air enters the disc eye, with the air flowing along the +z axis. The average flow rate of the air dissipated from the ventilation channels is calculated to be 180.96 m/s. However, despite this relatively high flow rate, the average velocity of the brake pad region remains considerably low at 18.32 m/s. This observation highlights the inadequate cooling provided to a crucial component of the wheel assembly. Examining the side view of the wheel hub, depicted in the accompanying figure, reveals the presence of relatively low velocities, particularly in the -y direction. This indicates that the airflow in this region is not effectively contributing to the cooling of the brake disc and ventilation channels. To address this cooling deficiency and ensure proper cooling for the brake disc and ventilation channels, it is necessary to enhance the -y component of the air velocity. By increasing the airflow in this direction, a greater amount of cooling air can be directed towards the brake disc and the ventilation channels, mitigating the risk of overheating and enhancing the overall performance and safety of the braking system.

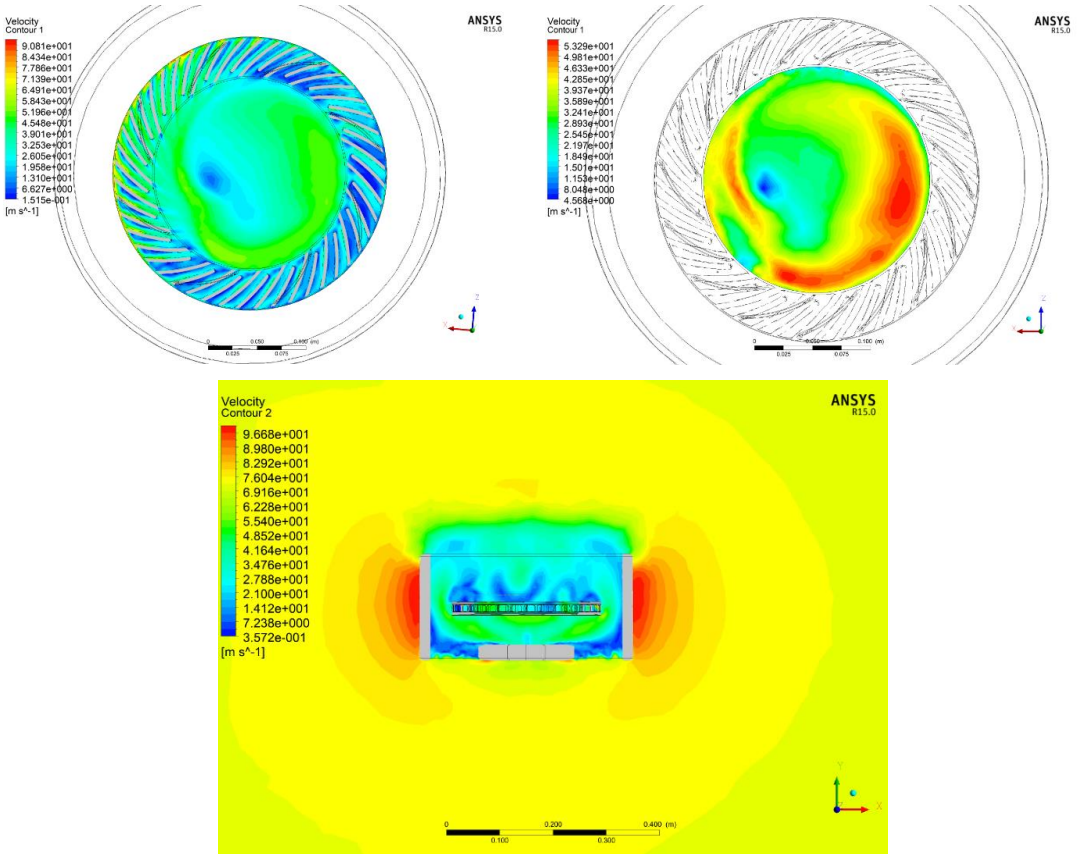

Figure 26 No duct case. Figure 26a (top left) shows the velocity contours at the ventilation channels. Figure 26b (top right) shows the velocity contours at the "eye" of the brake disc. Figure 26c (bottom) shows the side view of the wheel hub.

Table 3 Vane velocities for ductless design

Vanes Velocities (m/s)	
Average Velocity (m/s)	20.71
Flow rate (L/s)	180.96

Table 4 Incidence velocities for ductless design

Vanes inlet	
Min Velocity (m/s)	4.58
Max Velocity (m/s)	55.03
Average Velocity (m/s)	37.51
Brake pad region	
Min Velocity (m/s)	1.86
Max Velocity (m/s)	51.39
Average Velocity (m/s)	18.32

3.2 Duct with a 90° angle outlet

The following figure can provide us with valuable information regarding the way the air from the duct outlets, reacts with the air circulating the rotor region. The pictures on the second row, depict the velocity contours at the middle of the bottom (left) and top (right) ducts. It seems that the air coming out of the ducts cannot “reach” the brake rotor properly. We will discuss further this topic on the next section of this thesis, as it provides the groundwork for future designs and applications.

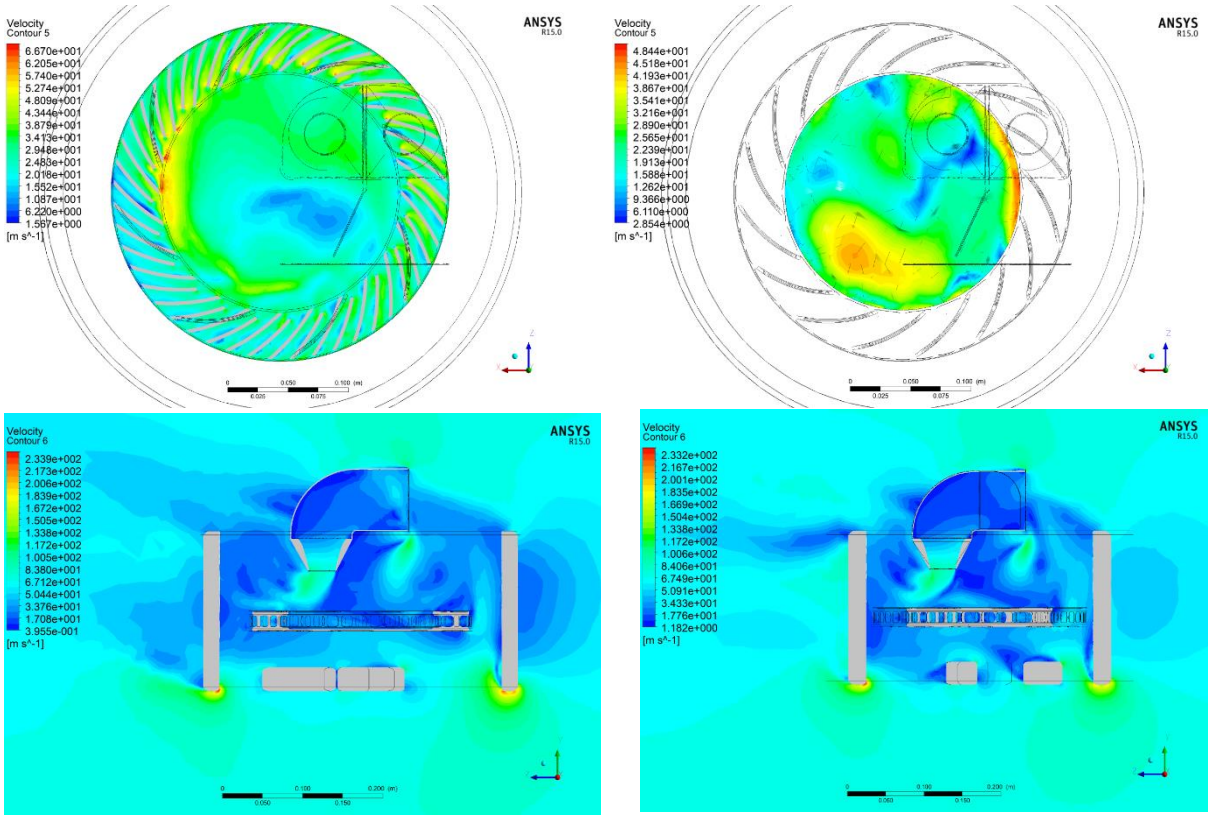

Figure 27 90° duct case. Figure 27a (top left) shows the velocity contours at the ventilation channels. Figure 27b (top right) shows the velocity contours at the “eye” of the brake disc. Figures 27c and 27d (bottom left and right respectively) show the velocity contours at the centre of the duct bottom and top outlet respectively.

Table 5 Outlet velocities for 90° duct.

	Flap angle = -25°	Flap angle = 0°	Flap angle = +25°
Upper outlet			
Average Velocity (m/s)	84.21	81.32	86.03

Flow rate (L/s)	4.1	3.96	4.19
Lower Outlet			
Average Velocity (m/s)	83.23	81.27	79.44
Flow rate (L/s)	4.06	3.96	3.87

Table 6 Incidence velocities for 90° duct.

	Flap angle = -25°	Flap angle = 0°	Flap angle = +25°
Vanes inlet			
Min Velocity (m/s)	3.21	2.32	2.85
Max Velocity (m/s)	52.41	53.21	50.1
Average Velocity (m/s)	26.5	27.54	25.91
Brake pad region			
Min Velocity (m/s)	2.11	1.98	2.3
Max Velocity (m/s)	87.32	86.95	87.8
Average Velocity (m/s)	45.36	40.87	38.54

Table 7 Vane velocities for 90° duct.

	Flap angle = -25°	Flap angle = 0°	Flap angle = +25°
Average Velocity (m/s)	28.36	28.12	27.72
Flow rate (L/s)	248.16	246.24	242.4

3.3 Duct with a 70° flap angle outlet

In the following figure, we are starting to see the advantages of an angled duct outlet, since it can provide the brake pad region with extra airflow. The average speed of the brake pad region is significantly increased (>30%) compared with the no duct and 90° duct cases. The increased airflow emerging from the lower duct is effectively channeled towards the brake rotor, optimizing its directionality. Within the wheel region, substantial pressure variations are encountered, necessitating the careful placement of the exiting duct airflow in close proximity to the brake disc to minimize disturbances and maximize its advantageous effects.

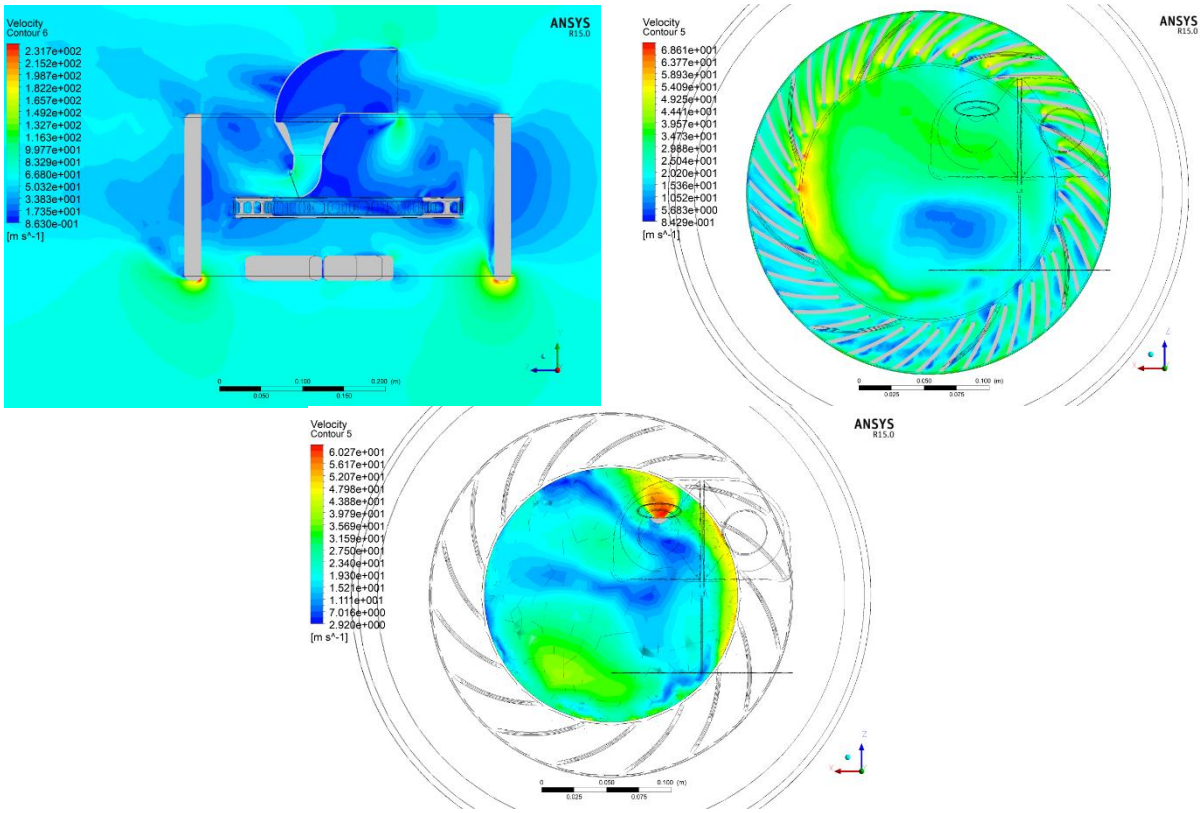

Figure 28 Duct with 70° angle case. Figure 28a (top left) shows the velocity contours at the centre of the angled duct outlet. Figure 28b (top right) shows the velocity contours at the ventilation channels. Figure 28c (bottom) shows the velocity contours at the "eye" of the brake disc.

Table 8 Outlet velocities for 70° duct.

	Flap angle = -25°	Flap angle = 0°	Flap angle = +25°
Upper outlet			
Average Velocity (m/s)	85.29	86.88	85.81
Flow rate (L/s)	4.16	4.23	4.18
Lower Outlet			
Average Velocity (m/s)	73.71	71.41	72.99
Flow rate (L/s)	3.59	3.49	3.56

Table 9 Incidence velocities for 70° duct.

	Flap angle = -25°	Flap angle = 0°	Flap angle = +25°
Vanes inlet			
Min Velocity (m/s)	1.2	2.92	3.15
Max Velocity (m/s)	63.55	62.31	63.64
Average Velocity (m/s)	26.9	26.94	27.34
Brake pad region			
Min Velocity (m/s)	6.34	6.59	6.1
Max Velocity (m/s)	95.45	93.34	95.34
Average Velocity (m/s)	62.44	57.68	55.12

Table 10 Vane velocities for 70° duct.

	Flap angle = -25°	Flap angle = 0°	Flap angle = +25°
Average Velocity (m/s)	26.32	27.88	28.38
Flow rate (L/s)	230.4	243.84	248.16

3.4 Duct with a 60° flap angle outlet

A 60° outlet provides an airflow more parallel to the car's direction, thus increasing the velocity at the brake pad region. By examining the air flow at the disc "eye", we can clearly see the decrease in the average velocity, mainly because, compared with the no duct case, we introduced a relatively large component between the free stream and the brake rotor. This decrease in air velocity might seem unwanted at first glance, but by applying small tweaks in the duct design, we can create a situation that works towards the better cooling of the rotor.

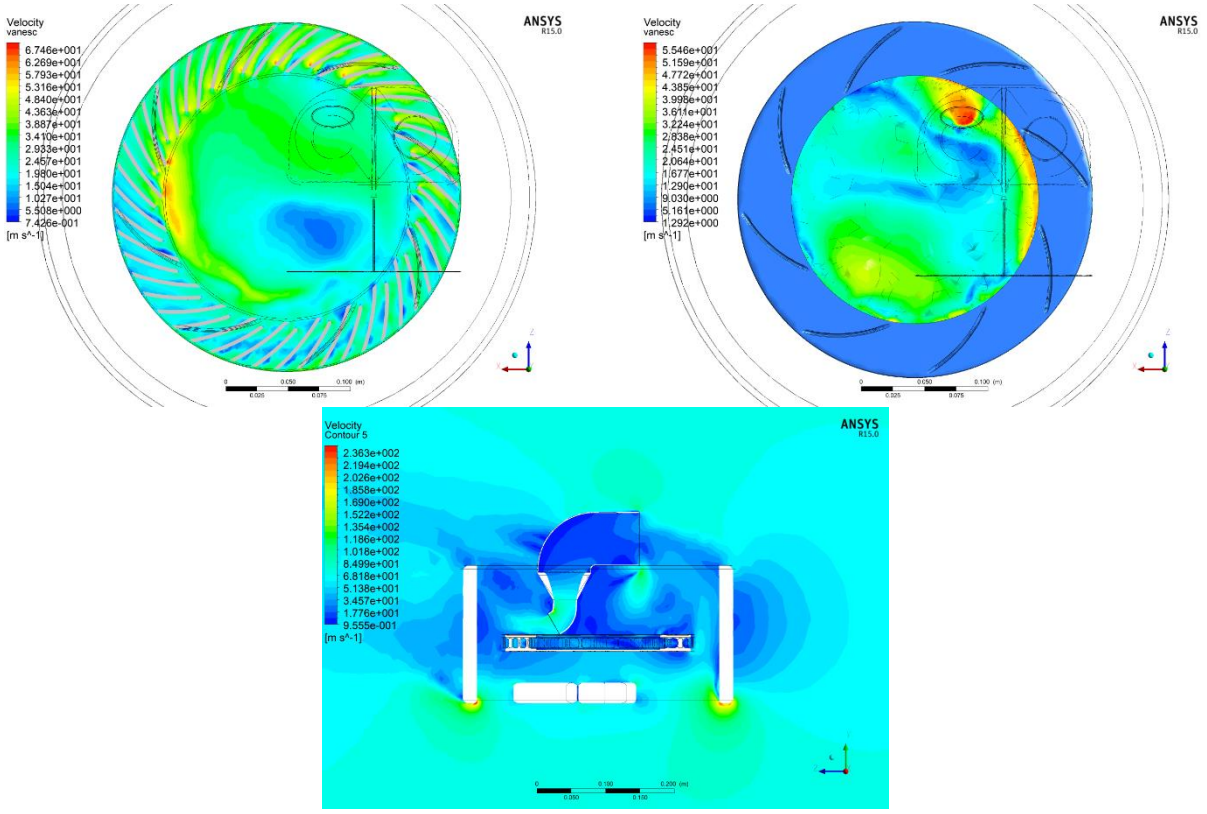

Figure 29 Duct with 60° angle case. Figure 29a (top right) shows the velocity contours at the ventilation channels. Figure 29b (top left) shows the velocity contours at the "eye" of the brake disc. Figure 29c (bottom) shows the velocity contours at the centre of the angled duct outlet.

Table 11 Outlet velocities for 60° duct.

	Flap angle = -25°	Flap angle = 0°	Flap angle = +25°
Upper outlet			
Average Velocity (m/s)	90.00	87.4	86.6
Flow rate (L/s)	4.38	4.26	4.22
Lower Outlet			
Average Velocity (m/s)	68.00	70.8	73.1
Flow rate (L/s)	3.31	3.45	3.56

Table 12 Incidence velocities for 60° duct.

	Flap angle = -25°	Flap angle = 0°	Flap angle = +25°
Vanes inlet			
Min Velocity (m/s)	0.44	1.29	1.83
Max Velocity (m/s)	58.80	57.39	59.86
Average Velocity (m/s)	25.62	26.25	25.94
Brake pad region			
Min Velocity (m/s)	7.4	9.09	6.23
Max Velocity (m/s)	93.08	93.45	96.41
Average Velocity (m/s)	63.89	57.43	56.34

Table 13 Vane velocities for 60° duct.

	Flap angle = -25°	Flap angle = 0°	Flap angle = +25°
Average Velocity (m/s)	30.28	31.15	32.13
Flow rate (L/s)	264.96	272.64	281.28

3.5 Duct with a 50° flap angle outlet

At 50° we do expect an increase in both the brake pad region and the ventilation channels. The airflow exiting the bottom duct as shown above, is slightly decreased, mainly because of the “sharper” turn the duct has to perform in order for the outlet to be at 50° flap angle. This is to be expected and in race car design, compromises like that, are always present.

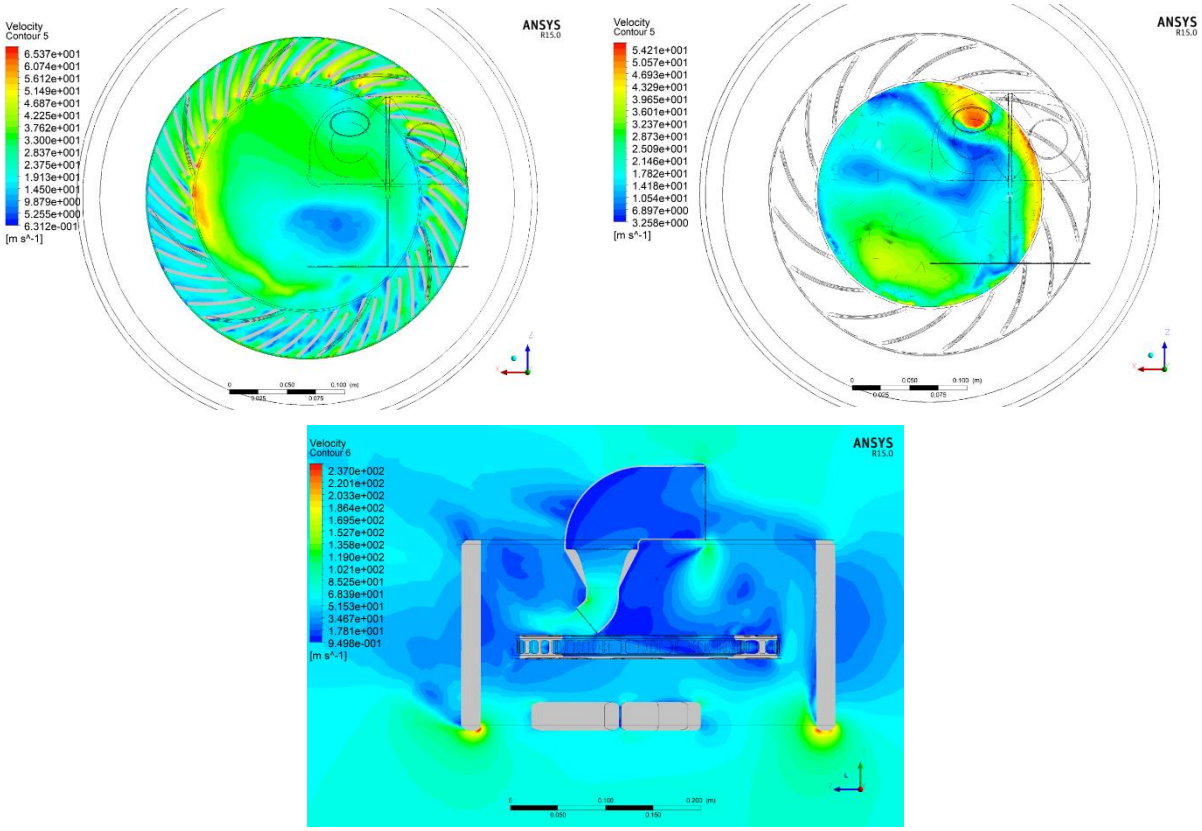

Figure 30 Duct with 50° angle case. Figure 30a (top right) shows the velocity contours at the ventilation channels. Figure 30b (top left) shows the velocity contours at the “eye” of the brake disc. Figure 30c (bottom) shows the velocity contours at the centre of the angled duct outlet.

Table 14 Outlet velocities for 50° duct.

	Flap angle = -25°	Flap angle = 0°	Flap angle = +25°
Upper outlet			
Average Velocity (m/s)	87.52	86.2	86.15
Flow rate (L/s)	4.26	4.2	4.2
Lower Outlet			
Average Velocity (m/s)	70.26	76.1	76.07
Flow rate (L/s)	3.42	3.71	3.71

Table 15 Incidence velocities for 50° duct.

	Flap angle = -25°	Flap angle = 0°	Flap angle = +25°
Vanes inlet			
Min Velocity (m/s)	2.75	3.26	2.56
Max Velocity (m/s)	54.2	56.03	56.99
Average Velocity (m/s)	24.87	25.53	25.53
Brake pad region			
Min Velocity (m/s)	8.97	9.60	9.67
Max Velocity (m/s)	95.63	96.89	99.91
Average Velocity (m/s)	64.13	60.18	57.31

Table 16 Vane velocities for 50° duct.

	Flap angle = -25°	Flap angle = 0°	Flap angle = +25°
Average Velocity (m/s)	26.3	27.30	29.56
Flow rate (L/s)	229.92	239.04	258.72

3.6 Comparison tables and data evaluation

We carried out 13 different simulations, for the no duct scenario and the duct with different outlet angles (90, 70, 60 and 50 degrees), in relation to the disc face scenario. From these simulations we are able to extract meaningful results about the importance and performance of the brake duct we designed. As shown in the previous section, using velocity contours we are able to evaluate with a visual aid the performance of the duct. Our main goal is to maximize the velocity in the brake pad region and the ventilation channels. If our brake duct was not active, we would have to select a specific angle for the inner flap and that would not be able to be changed, over the course of a race. By using an active brake duct, we are able to maximize the combination of the two velocities we are interested in.

To better evaluate the results, the velocities at the brake pad region (red square), at the ventilation channels (2cm radially before the outlet, green square) and at the duct outlet (5mm from the lip, yellow square) will be presented in a table form below. Also, a figure with the locations of the measurements is provided:

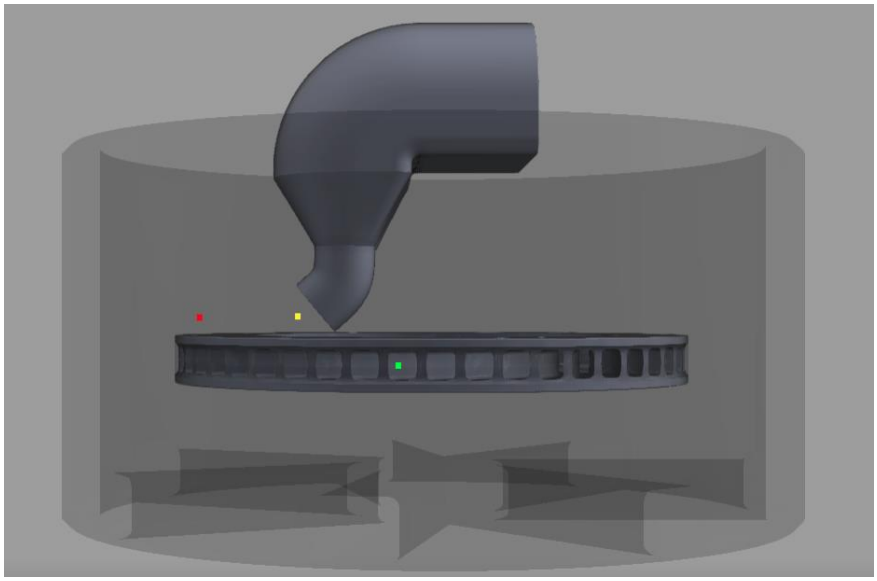

Figure 31 Measurement locations

Table 18 Average velocity (m/s) comparison with a 0° flap angle.

	No duct		90°		70°		60°		50°	
Vanes inlet	37.51	0%	27.54	-27%	26.94	-28%	26.25	-30%	25.53	-32%
Brake pad region	18.32	0%	40.87	123%	57.68	215%	57.43	213%	60.18	228%
Vanes Velocities	20.71	0%	28.12	36%	27.88	35%	31.15	50%	27.3	32%

Table 17 Average velocity (m/s) comparison with a -25° flap angle.

	No duct		90°		70°		60°		50°	
Vanes inlet	37.51	0%	26.5	-29%	26.9	-28%	25.62	-32%	24.87	-34%
Brake pad region	18.32	0%	45.36	148%	62.44	241%	63.89	249%	64.13	250%
Vanes Velocities	20.71	0%	28.36	37%	26.32	27%	30.28	46%	26.3	27%

Table 19 Average velocity (m/s) comparison with a +25° flap angle.

	No duct		90˚		70˚		60˚		50˚	
Vanes inlet	37.51	0%	25.91	-31%	27.34	-27%	25.94	-31%	25.53	-32%
Brake pad region	18.32	0%	38.54	110%	55.12	201%	56.34	208%	57.31	213%
Vanes Velocities	20.71	0%	27.72	34%	28.38	37%	32.13	55%	29.56	43%

First of all, the advantages of using a brake duct are clear by just comparing the velocity values for the three regions in question. With this brake duct design, we managed to significantly increase the velocity in the ventilation channels by using a duct with a flat flap. In the case of the 90° duct, an increase at an average of 35.67%. Similar findings can be observed for the 70° duct with an increase of 33%, 50.33% for the 60° duct and finally, 34% for the 50° duct. Over the course of a race which can last depending on the motorsport category, anywhere between 200 and 1000 kilometers in most cases, that increase can play a significant role and change the course of someone's race. By being able to monitor and keep the temperature of the brake rotor inside the suggested range, one can increase the lifetime of the rotors and the performance of the car. Another interesting find is related to the angle of the flap itself. We decided to test 3 different positions. At 0° (parallel to the road) and at +-25°. The side with the bigger air supply affects the different regions at a greater scale. As mentioned before, we are able to see the effect of the distance between the duct outlet and the brake disc by examining the velocity contours (see section 3.3). It is very important to keep a small distance between these two components, in order to maximize the cooling effects. By using an angled duct outlet, we are able to direct the air very close to the region of interest. We do have to keep in mind that the brake disc can reach temperatures of up to 1000°C. At those temperatures, the heating of the duct due to radiation should be considered. Usually, brake ducts are made from carbon fiber and so they can endure these temperatures. That is not always the case, so the brake ducts should be placed accordingly. In all different scenarios we are able to see the benefits of the shape of the duct outlet since a converging nozzle shape provides the acceleration in the flow needed to achieve high speeds. The outlet velocities tables provide us with that information, with the average velocity normal to the duct outlet being above 80 m/s (288 kph) in most scenarios. Finally, the angle of the duct outlet seems to affect more the brake pad region and less the ventilation channels. More figures of all the different scenarios can be examined in Appendix A. Let's take a look at the following charts.

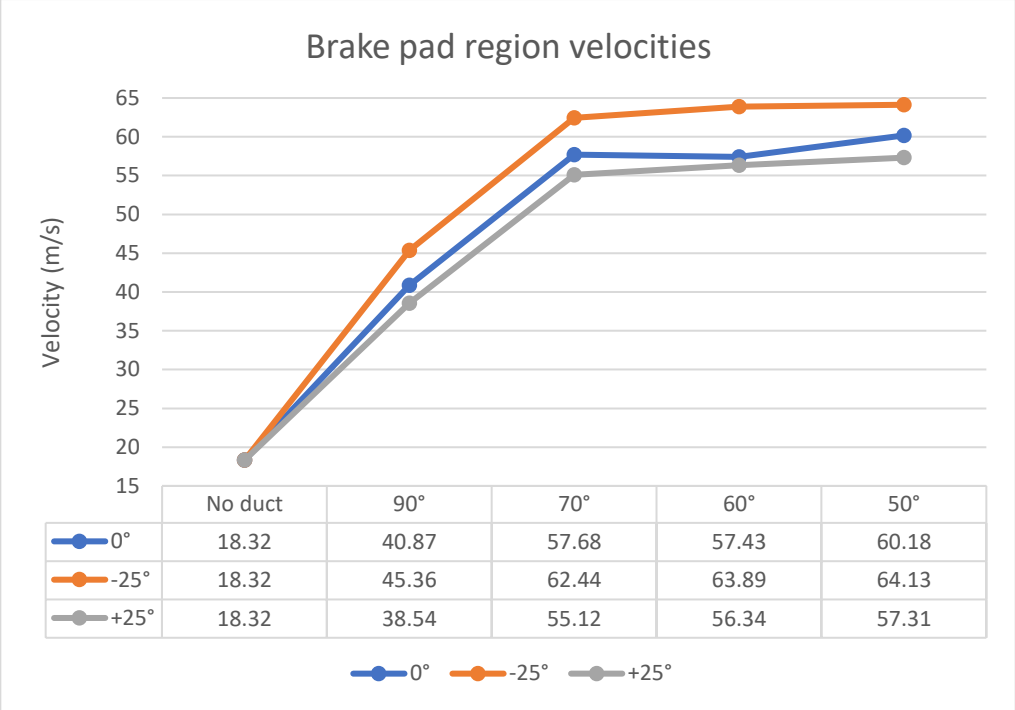

	No duct	90°	70°	60°	50°
0°	18.32	40.87	57.68	57.43	60.18
-25°	18.32	45.36	62.44	63.89	64.13
+25°	18.32	38.54	55.12	56.34	57.31

Figure 32 Brake pad region velocities chart.

When the flap is at a -25° angle, more airflow is directed towards the bottom (angled) duct outlet. The brake pad region cooling benefits from that, as the average velocity is higher in all different scenarios. By lowering the flap, we increased the brake pad region velocity by an average of 27.25% across all scenarios. In the case of the 60° duct, the increase was nearly 35%, showing that the combination of the two clearly works very well. We were able to triple the velocity of the brake pad region in most cases with average speeds reaching nearly 65m/s, compared with 18m/s with the no duct case.

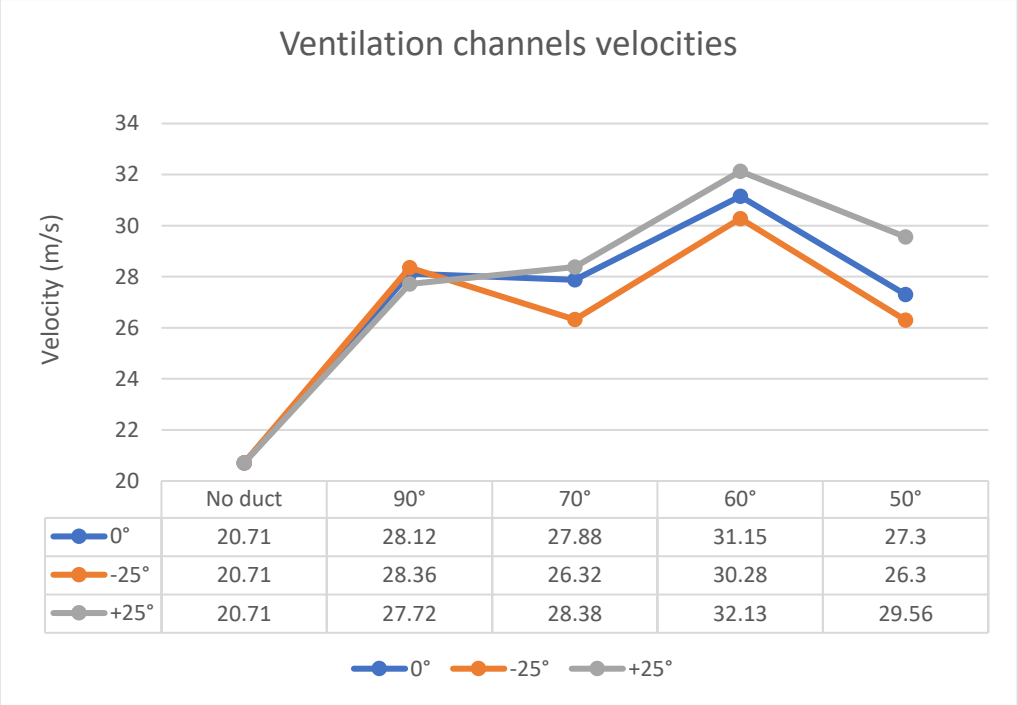

Figure 33 Ventilation channels velocities chart.

Furthermore, and by examining the above figure, we are able to measure the expected increase in the average velocity of the ventilation channels, since more air is directed towards them when the flap is moved up 25 degrees. The grey line depicts exactly that. On average we managed to increase the velocity of the ventilation channels by 42.25% and in some cases (60° duct), by over 50%. Simultaneously, when the flap is lowered a decrease in ventilation channel velocity is presented. This is not only expected but the duct was designed in order to provide the performance needed in all configurations. If the engineers want to increase cooling in the brake pad region, they also want to decrease the cooling on the ventilation channels in order to avoid a large decrease of temperature. Such a decrease would result in a very cool rotor which will not be able to provide the required stopping power at the next braking point, thus worsening the performance of the car. It is important to note the increase in ventilation channel speeds in terms of airflow rate. We were able to calculate the average airflow rate in Liters per second in all different scenarios tested. A table containing the results is provided below:

Table 20 Average flow rate of the ventilation channels

	Flow rate (L/s)
No duct	180.96
90° (-25°, 0°, +25°)	248.16
	246.24
	242.4
70° (-25°, 0°, +25°)	230.4
	243.84
	248.16
60° (-25°, 0°, +25°)	264.96
	272.64
	281.28
50° (-25°, 0°, +25°)	229.92
	239.04
	258.72

At high speeds, the ventilation channels of the brake discs go through vast amounts of air volume. A single rotor as shown above can handle over 200 liters per second. Over the course of a race, the four rotors will dissipate heat mainly through the ventilation channels since racing cars can easily reach speeds of 200 or even 300kph each lap.

The position of the flap plays a significant role in the air supply in different regions of the brake assembly, thus, the possibilities for the race mechanics of a racing team are endless. One could direct more air in the pad region of the disc in order to cool down the different components of the brake assembly. At the start of a big straight, the brake duct could be programmed to provide all the possible air supply to the ventilation channels in order to maximize the cooling of the disc itself. When the temperature of the brake disc drops below a specified value, the air could be directed to a different region, to maintain the discs inside their working temperature region.

Further development of an active brake duct could result in more ways to cool down the vital regions of the wheel assembly. More specifically, we could design a movable outlet, thus increasing the degree of freedom for the race car engineers. We would be able to monitor the temperatures by directing the air that comes out of the duct. From this study, the benefits of an angled outlet towards the brake pad region are very clear. But what if the outlet was angled in the opposite direction i.e. opposite to the moving direction. Maybe, we would be able to further increase the ventilation channel velocity. Another possible way to increase a brake duct's cooling capabilities is to intercept a radiator between the duct inlet and outlets. By doing so, we would be able to cool down the air, thus increasing the performance of the cooling assembly. Of course, such a device would result in a decrease of the

air velocity, so a real-life test should be carried out in order to determine the pros and cons of such an idea. Furthermore, we could expand the capabilities of the brake ducts as it can be used in more applications.

Firstly, the brake ducts are in a very prime position, airflow wise, in the car. If they are active, they can redirect the air in more than one region of the race car and not just the brakes. Engineers can set the ducts in a way to direct the airflow to the undertray of the race car. In race car design, the underbody of the car plays a vital role in the vehicle's aerodynamics. Air channels are designed to bring the air at the back of the car creating a low-pressure area that increases the car's downforce. This device is called a diffuser. Another possible use of a brake duct is the heating of the tires the racing car is using. Take the following situation as an example. During a race, the tires of the car, like the brakes, perform at their best when their temperature is inside a predefined temperature window. This window changes from tire to tire as it depends on the compound of the tire. A race car driver will drive in such a way to increase or decrease the temperatures of the tires. A driver can even affect the temperature of each individual tire independently. The above way of driving will cost the driver time because he or she will not be driving the car with the sole purpose of being as fast as possible around a corner. A way around this is the control of the tire temperature by using the brake ducts. If the driver needs the temperature of a specific tire to decrease, more air could be directed towards the tire profile via an active brake duct outlet. We could further develop this idea by exploring the heating of the tires as well.

When the temperature of the tires falls out of the specified range, the driver no longer has the amount of traction needed to "extract" the best performance from the car. Brake ducts could be designed in order to channel the air coming out of the disc ventilation channels towards the wheel rim. By doing so, hot air will heat up rim, which is already hot because of the radiation of the discs, and by doing so, the tires via conduction, will heat up.

It is very clear that in that small region of a racing car, so many different phenomena take place and at higher speeds the flow becomes very complicated. One of the limitations of this thesis is the lack of computational power. Being able to perform the aerodynamic analysis needed by using the sliding mesh method (transient simulation) would result in more accurate results. Also, due to the Covid-19 pandemic an experimental study, that would validate these results in a wind tunnel, could not be carried out. Nonetheless, this study provides the groundwork for the understanding of such devices and their importance in vehicle racing.

4. Conclusion

In this thesis, we managed to test the importance of brake ducts and the advantages of an active one. The applications of a brake duct are mainly race cars and high-performance road cars. We focused on open-wheel race cars, as the most extreme scenarios in terms of brake cooling come from that type of racing. Brake discs, under heavy and repetitive braking, can reach temperatures of up to 1000°C, so the teams and drivers are met with a difficult task. Trying to maintain the temperature of the brake discs and other components below a specific limit. Although there are different ways to cool the brakes, a brake duct will provide the best results for a reasonable price and great durability. Having a static brake duct, the racing team can only make one decision as to how to set up the cooling of the brakes. As a racing team, it is very important to always have different solutions to the same problem and being able to select the best one for a specific time frame. During a race, the cooling needs of the race car in general, but more specifically, the brakes, is always changing. The driver wants the best and most efficient cooling to extract 100% of the performance of the car. An active brake duct, where via sensors and a step motor, a moving flap changes the air supply to different brake compartments, can provide that ability to the driver and the team.

The design proposed turned out to increase the braking performance of a race vehicle in different areas of interest. A duct with a 60° bottom outlet can provide the wheel assembly with a 249% increase in brake pad region velocity and 55% increase in ventilation channel velocity. The use of a brake duct turns out to be very beneficial for the performance of a race car and racing teams should research and develop such devices. Also, federations, such as the Fédération Internationale de l'Automobile (FIA) should consider changing the technical regulations in different motorsports to allow more active aerodynamic elements, such as brake ducts. Future work should include even more radical brake duct designs that channel air to different parts of a race car. One example is the hot air coming out of the disc channels, which could be used to heat up the tires. An experimental test rig in the laboratory of fluid mechanics and turbomachinery where a spinning disc could be decelerated using brake calipers would create many research opportunities in the fields of Fluid mechanics and Heat transfer.

5. References

Adamowicz, A. and Grzes, P. (2011) 'Influence of convective cooling on a disc brake temperature distribution during repetitive braking', *Applied Thermal Engineering*, 31(14–15), pp. 2177–2185. Available at: https://doi.org/10.1016/j.applthermaleng.2011.05.016.

Anderson, J.D. (2011) *Fundamental of Aerodynamics*. 5th edn. New York: McGraw-Hill Book Company.

Belhocine, A. and Wan Omar, W.Z. (2018) 'Computational fluid dynamics (CFD) analysis and numerical aerodynamic investigations of automotive disc brake rotor', *Australian Journal of Mechanical Engineering*, 16(3), pp. 188–205. Available at: https://doi.org/10.1080/14484846.2017.1325118.

Bevilacqua, M., Babutskyi, A. and Chrysanthou, A. (2015) 'A review of the catalytic oxidation of carbon-carbon composite aircraft brakes', *Carbon*, 95, pp. 861–869. Available at: https://doi.org/10.1016/j.carbon.2015.08.100.

Björgum, O.B. (1961) 'Turbulence: Classic Papers on Statistical Theory (S. K. Friedlander and L. Topping, eds.)', *SIAM Review* [Preprint]. Available at: https://doi.org/10.1137/1003069.

Cengel, Y.A. and Cimbala, J.M. (2017) *FLUID MECHANICS: FUNDAMENTALS AND APPLICATIONS*.

Cruceanu, C. (2007) *Frâne Pentru Vehicle Feroviare [Brakes for Railway Vehicles]*.

Day, A.J. (1987) 'An analysis of speed, temperature, and performance characteristics of automotive drum brakes.', 110(April).

Deardorff, J.W. (1970) 'A numerical study of three-dimensional turbulent channel flow at large Reynolds numbers', *Journal of Fluid Mechanics*, 41(2), pp. 453–480. Available at: https://doi.org/10.1017/S0022112070000691.

Huang, P.G., Bradshaw, P. and Coakley, T.J. (1992) 'Assessment of closure coefficients for compressible-flow turbulence models', *Nasa Technical Memorandum* [Preprint], (October 1992).

Hudson, M.D. and Ruhl, R.L. (1997) 'Ventilated brake rotor air flow investigation', *SAE Technical Papers* [Preprint], (41 2). Available at: https://doi.org/10.4271/971033.

Jeong, B. *et al.* (2014a) 'Optimization of Cooling Air Duct and Dust Cover Shape for Brake Disc Best Cooling Performance', *SAE Technical Papers*, 2014-Septe(September). Available at: https://doi.org/10.4271/2014-01-2519.

Jeong, B. *et al.* (2014b) 'Optimization of Cooling Air Duct and Dust Cover Shape for Brake Disc Best Cooling Performance', in *SAE Technical Papers*. SAE International. Available at: https://doi.org/10.4271/2014-01-2519.

Jerhamre, A. and Bergström, C. (2001) 'Numerical study of brake disc cooling accounting for both aerodynamic drag force and cooling efficiency', *SAE Technical Papers* [Preprint], (724). Available at: https://doi.org/10.4271/2001-01-0948.

Johnson, D.A., Sperandei, B.A. and Gilbert, R. (2003) 'Analysis of the flow through a vented automotive brake rotor', *Journal of Fluids Engineering, Transactions of the ASME*, 125(6), pp. 979–986. Available at: https://doi.org/10.1115/1.1624426.

Kataoka, T. *et al.* (1991) 'Numerical simulation of road vehicle aerodynamics and effect of aerodynamic devices', *SAE Technical Papers* [Preprint]. Available at: https://doi.org/10.4271/910597.

Kolmogorov, A.N. (1941) 'The local structure of turbulence in incompressible viscous fluid for very large Reynolds numbers', *Doklady Akademii Nauk SSSR*, 30, pp. 299–303. Available at: https://doi.org/10.1098/rspa.1991.0075.

Lee, K. (1999) 'Numerical prediction of brake fluid temperature rise during braking and heat soaking', *SAE Technical Papers* [Preprint], (724). Available at: https://doi.org/10.4271/1999-01-0483.

Luiz Filipe de Medeiros Gomes *et al.* (2018) *Study of Temperature Reduction in Automobile Brake Discs by Forced Convection*.

M. K. Khalid, M. R. Mansor, S. I. Abdul Kudus, M. M. Tahir, and M.Z.H. (2011) 'Performance Investigation of the UTeM EcoCar Disc Brake System ', *International Journal of Engineering & Technology IJET-IJENS*, 11(6), pp. 1–6.

Maccormack, R.W. (1993) 'A perspective on a quarter century of CFD research', *11th Computational Fluid Dynamics Conference, 1993* [Preprint]. Available at: https://doi.org/10.2514/6.1993-3291.

McComb, W.D. (1990) *The physics of fluid turbulence*. New York: Oxford University Press Inc.

Menter, F. (1992) 'Improved two-equation k-omega turbulence models for aerodynamic flows', *NASA Technical Memorandum*, (103978), pp. 1–31.

Menter, F.R. (1994a) 'Two-equation eddy-viscosity turbulence models for engineering applications', *AIAA Journal*, 32(8), pp. 1598–1605. Available at: https://doi.org/10.2514/3.12149.

Menter, F.R. (1994b) 'Two-equation eddy-viscosity turbulence models for engineering applications', *AIAA Journal*, 32(8), pp. 1598–1605. Available at: https://doi.org/10.2514/3.12149.

Nieuwstadt, F.T.M. *et al.* (1994) 'Direct and large-eddy simulations of turbulence in fluids', *Future Generation Computer Systems* [Preprint]. Available at: https://doi.org/10.1016/0167-739X(94)90018-3.

Patil, H. *et al.* (2021) 'CFD simulation model for mixing tank using multiple reference frame (MRF) impeller rotation', *ISH Journal of Hydraulic Engineering*, 27(2), pp. 200–209. Available at: https://doi.org/10.1080/09715010.2018.1535921.

Pearson, S.R. *et al.* (2013) 'The effect of temperature on wear and friction of a high strength steel in fretting', *Wear*, 303(1–2), pp. 622–631. Available at: https://doi.org/10.1016/j.wear.2013.03.048.

Reynolds, O. (1895) 'On the Dynamical Theory of Incompressible Viscous Fluids and the Determination of the Criterion.', *Philosophical Transactions of the Royal Society A: Mathematical, Physical and Engineering Sciences*, 10(186(0)), pp. 123–164.

Shang, J.S. (2004) 'Three decades of accomplishments in computational fluid dynamics', *Progress in Aerospace Sciences*, 40(3), pp. 173–197. Available at: https://doi.org/10.1016/j.paerosci.2004.04.001.

Smagorinsky, J. (1963) 'General circulation experiments wiht the primitive equations I. The basic experiment', *Monthly Weather Review*, 91(3), pp. 99–164. Available at: https://doi.org/10.1126/science.27.693.594.

Valvano, T. and Lee, K. (2000) 'An analytical method to predict thermal distortion of a brake rotor', *SAE Technical Papers* [Preprint], (724). Available at: https://doi.org/10.4271/2000-01-0445.

Vincenti, B.W.G. *et al.* (1956) *Calculations of the Flow Over an Inclined Flat Plate at free Stream Mach Number 1*. Washington.

Voller, G.P. *et al.* (2003) 'Analysis of automotive disc brake cooling characteristics', *Proceedings of the Institution of Mechanical Engineers, Part D: Journal of Automobile Engineering*, 217(8), pp. 657–666. Available at: https://doi.org/10.1243/09544070360692050.

Wilcox, D.C. (1988) 'Reassessment of the scale-determining equation for advanced turbulence models', *AIAA Journal*, 26(11), pp. 1299–1310. Available at: https://doi.org/10.2514/3.10041.

Yadav, S. and Lanfrit, M. (2005) *Best practice guidelines for handling Automotive External Aerodynamics with FLUENT*.

Zhang, Z. *et al.* (2007) 'Evaluation of various turbulence models in predicting airflow and turbulence in enclosed environments by CFD: Part 2—comparison with experimental data from literature', *HVAC and R Research*, 13(6), pp. 871–886. Available at: https://doi.org/10.1080/10789669.2007.10391460.

6. Appendix A

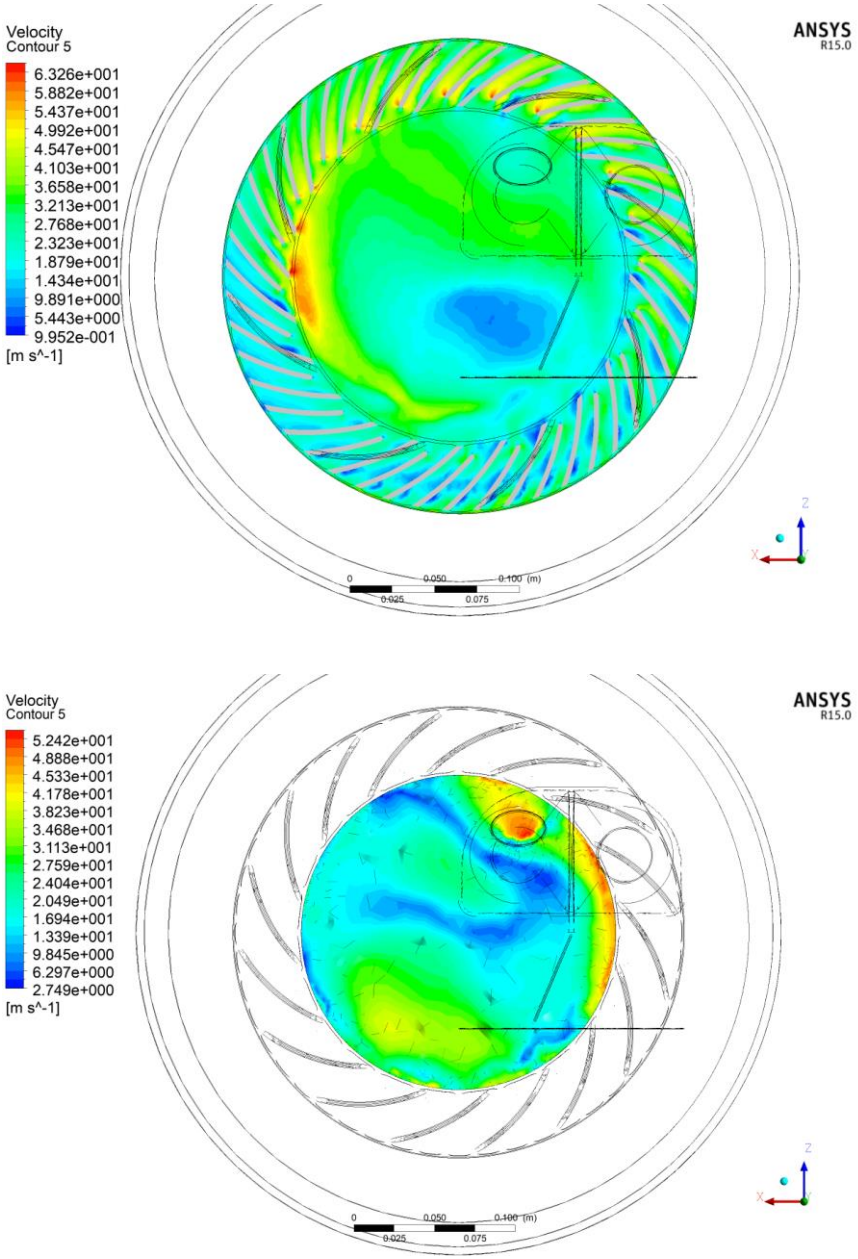

Figure 34 Duct with 50° angle and -25° flap.

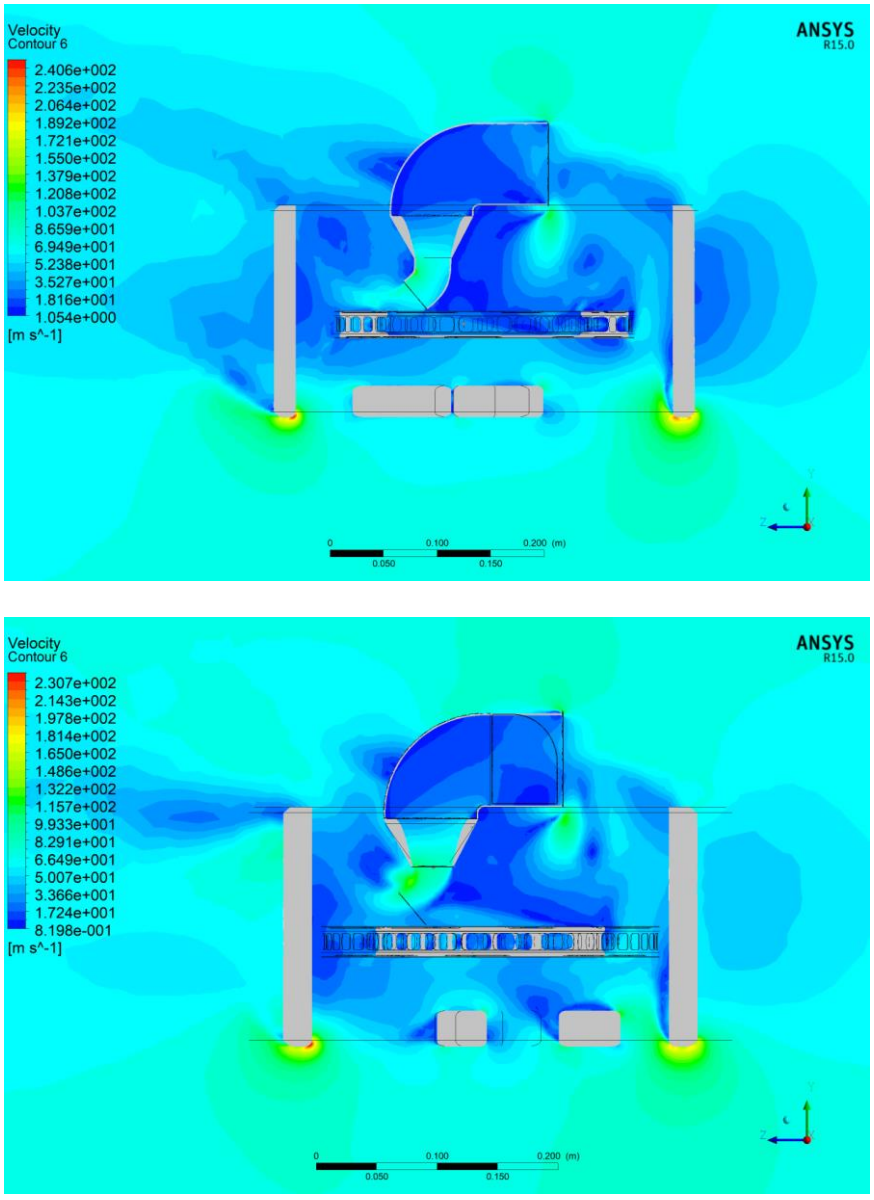

Figure 35 Bottom and Top duct outlet (50°, -25° flap).

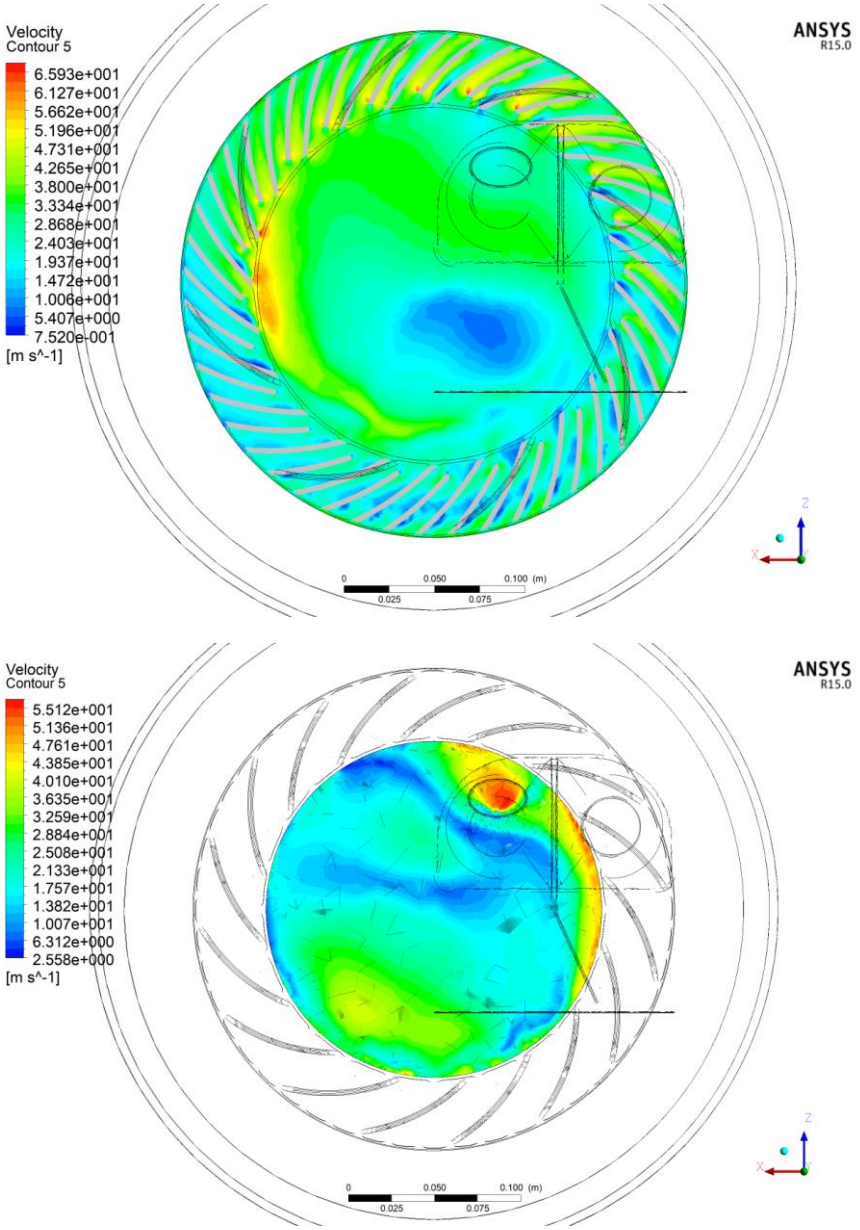

Figure 36 Duct with 50° angle and +25° flap.

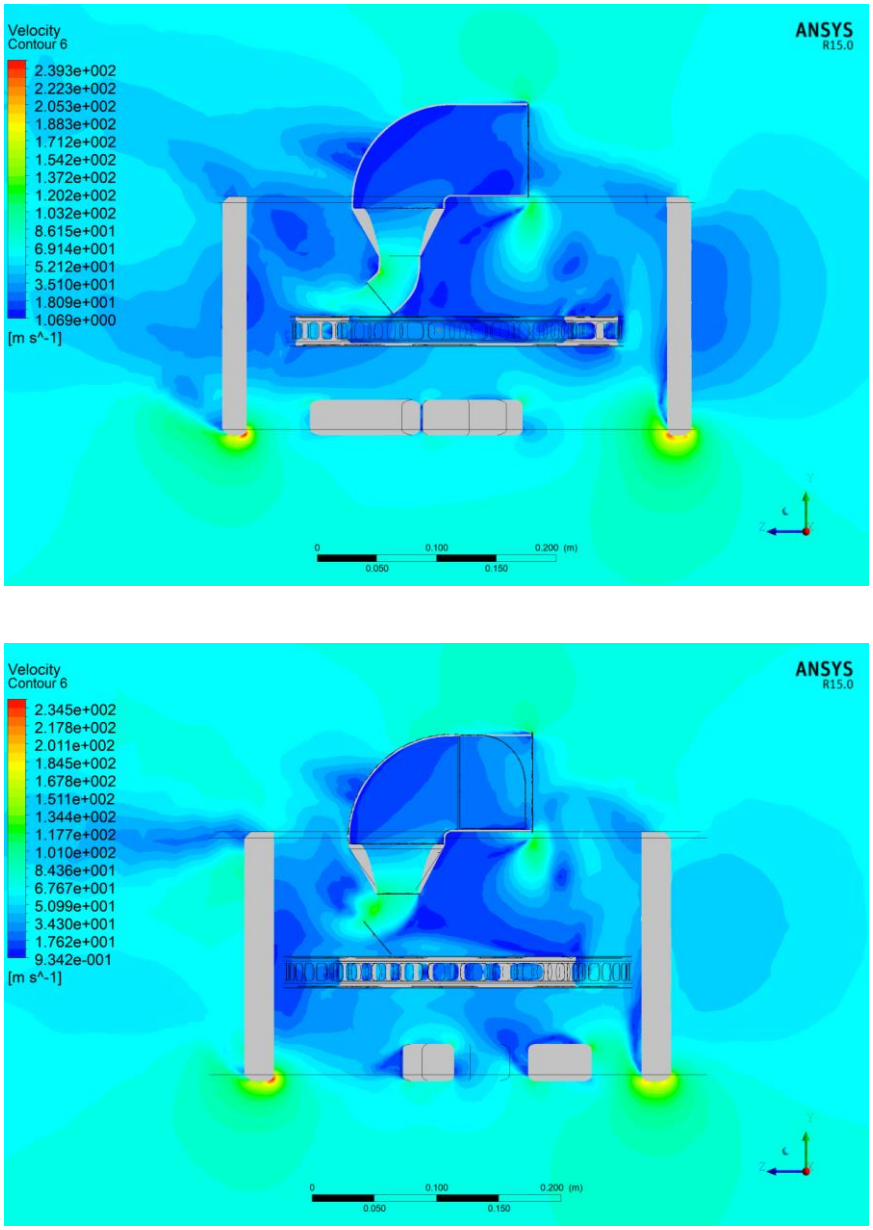

Figure 37 Bottom and Top duct outlet (50°, +25° flap).

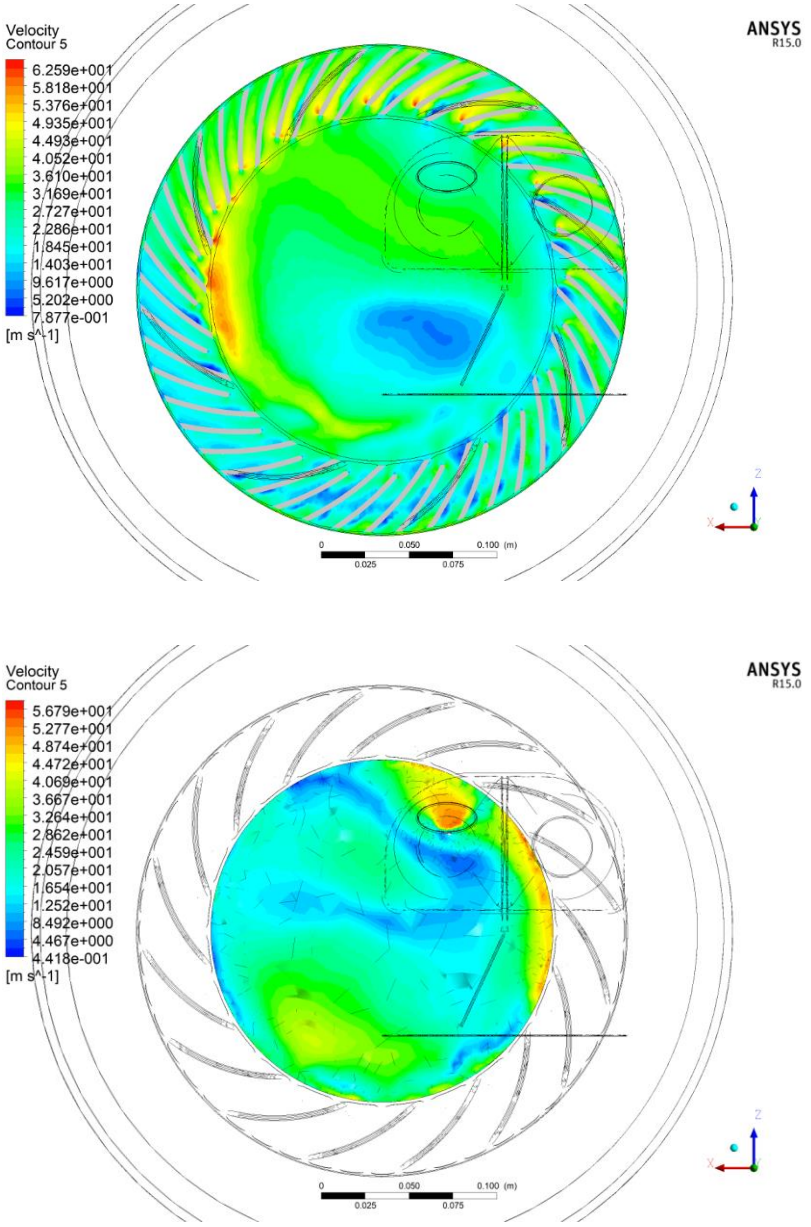

Figure 38 Duct with 60° angle and -25° flap.

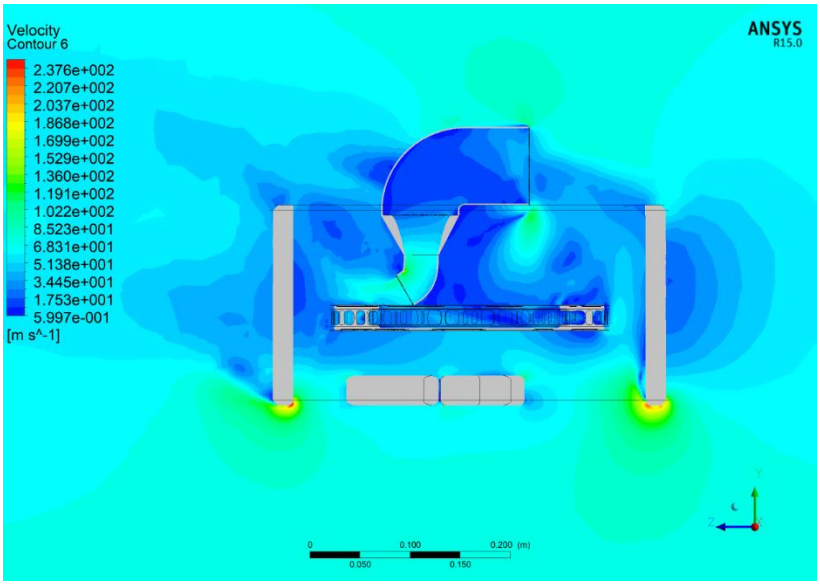

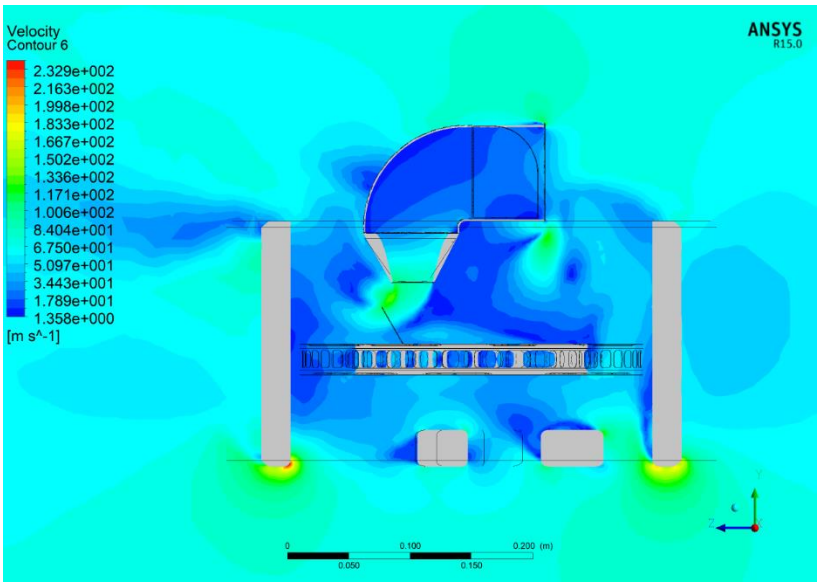

Figure 39 Bottom and Top duct outlet (60°, -25° flap).

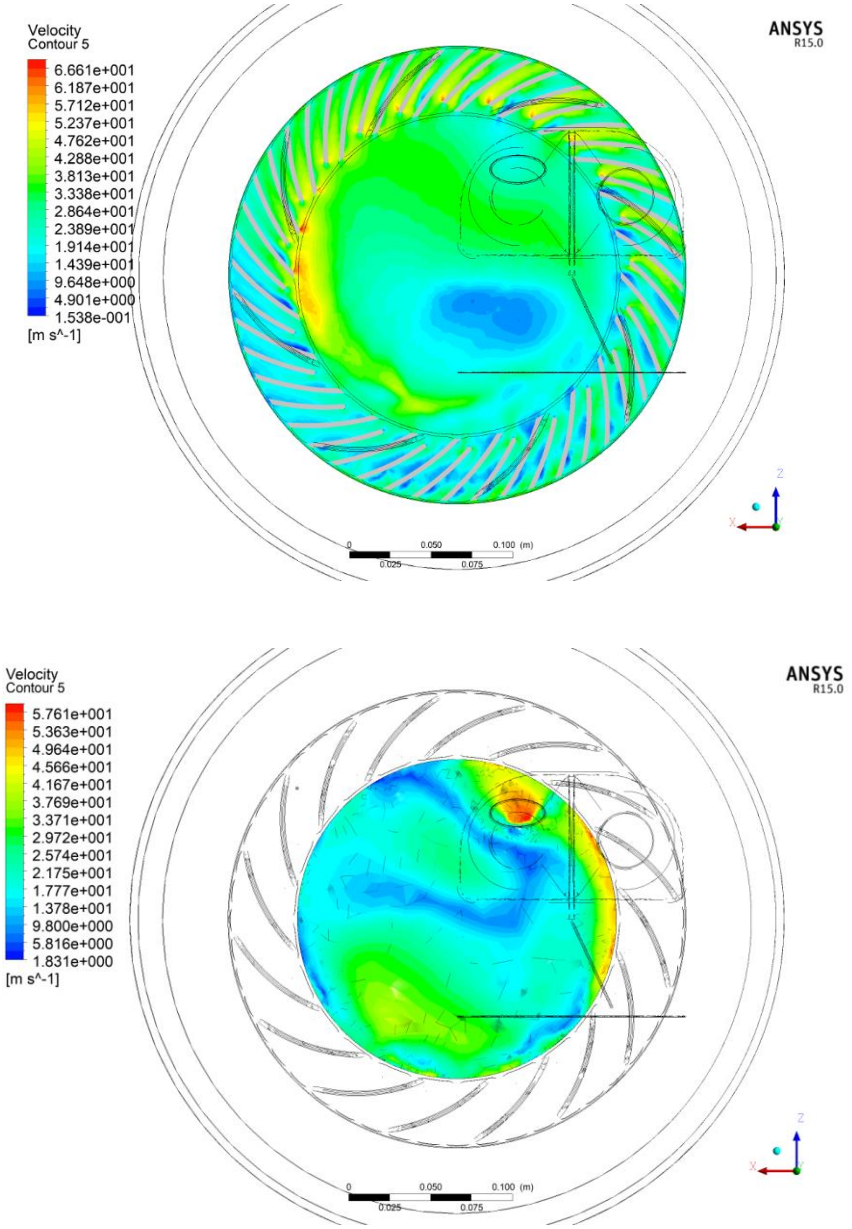

Figure 40 Duct with 60° angle and +25° flap.

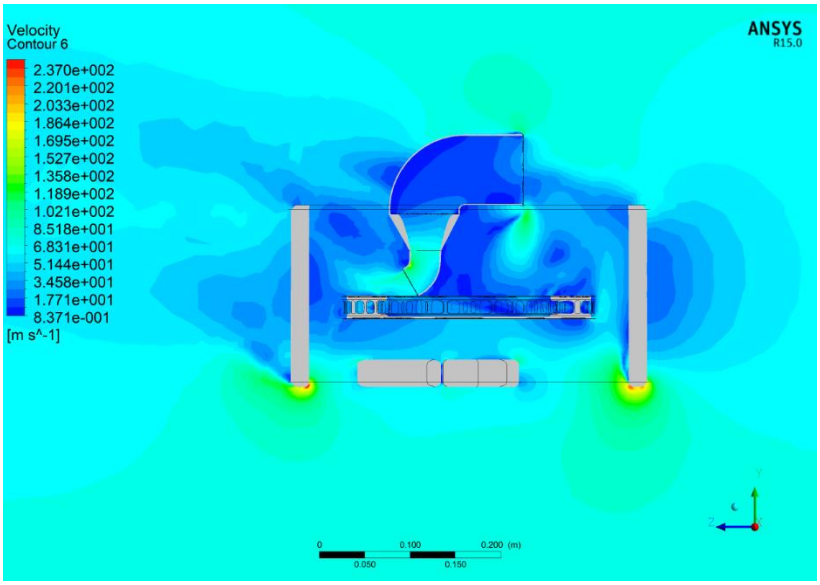

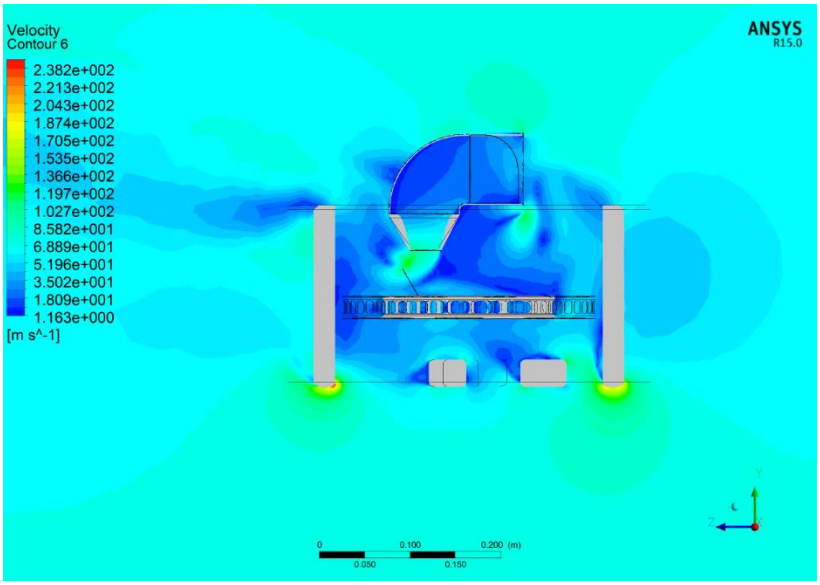

Figure 41 Bottom and Top duct outlet (60°, +25° flap).

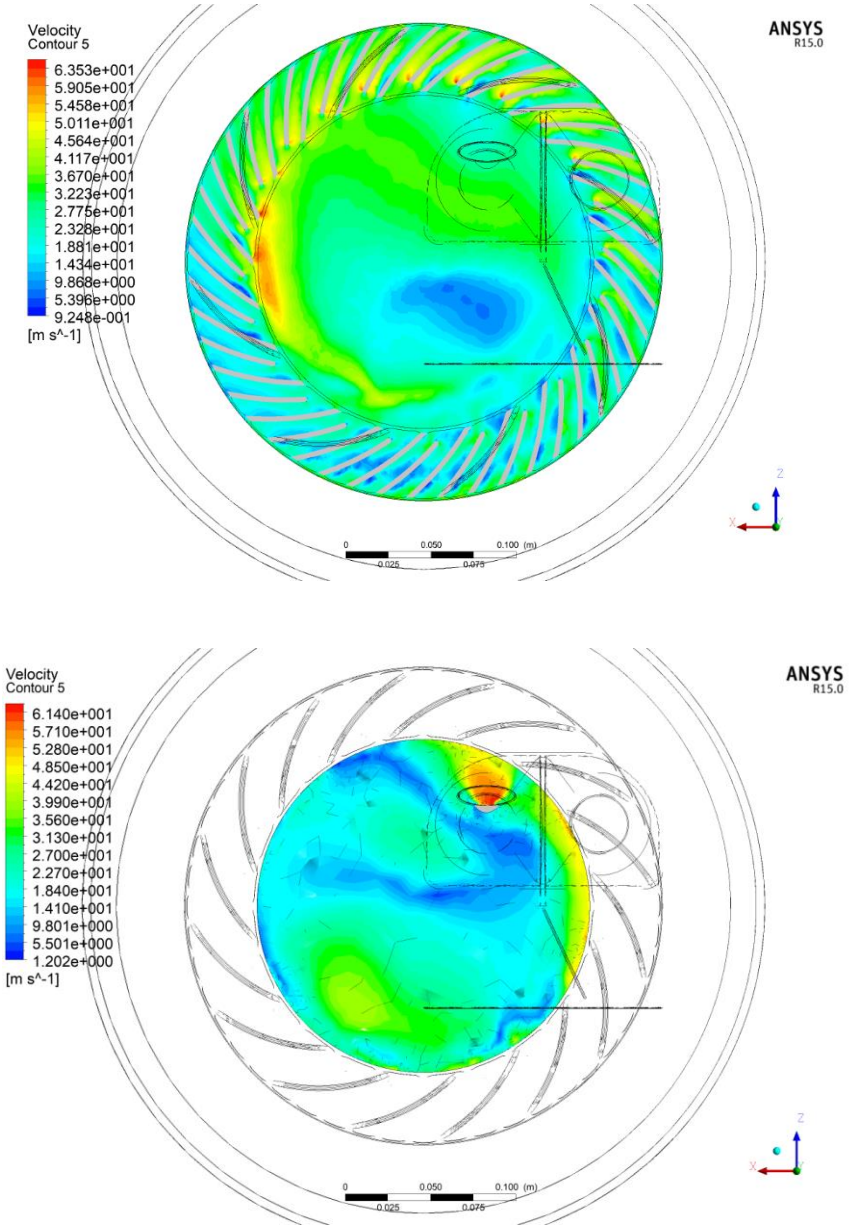

Figure 42 Duct with 70° angle and -25° flap.

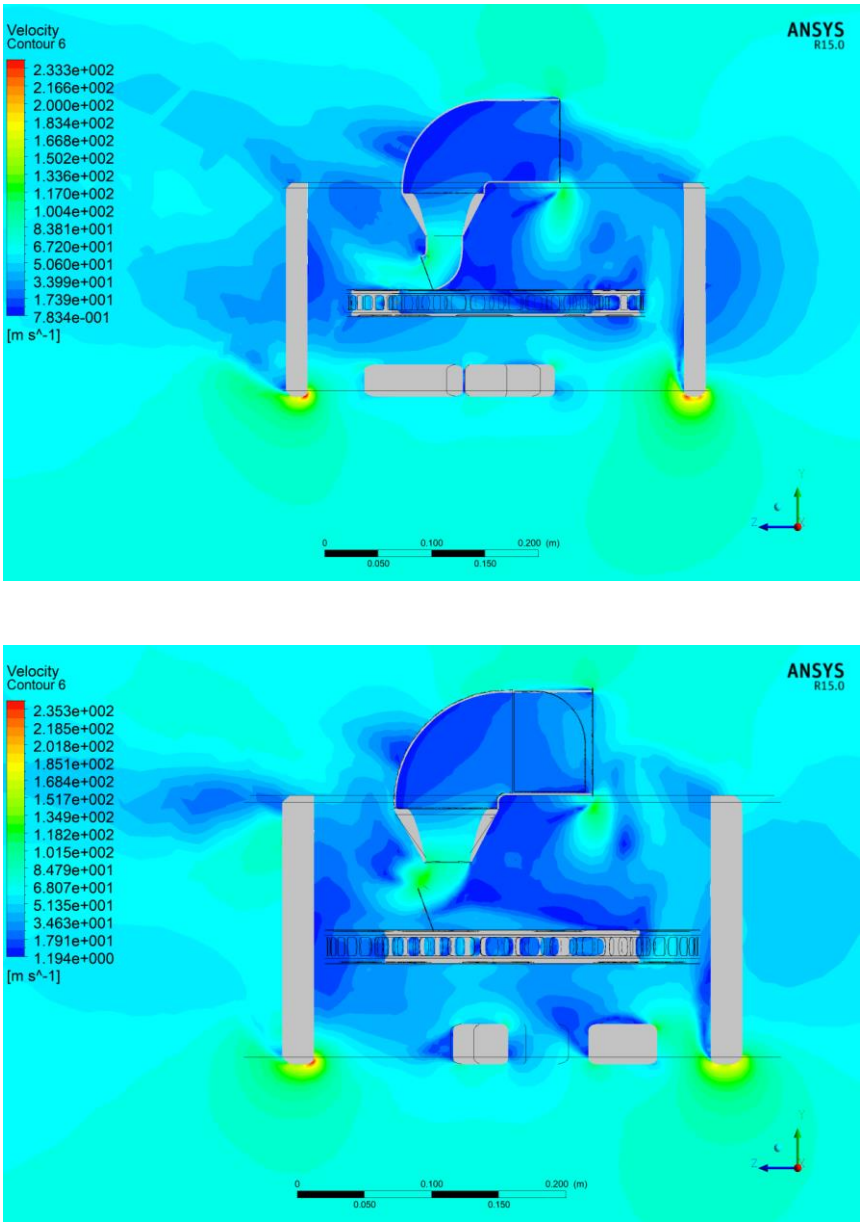

Figure 43 Bottom and Top duct outlet (70°, -25° flap).

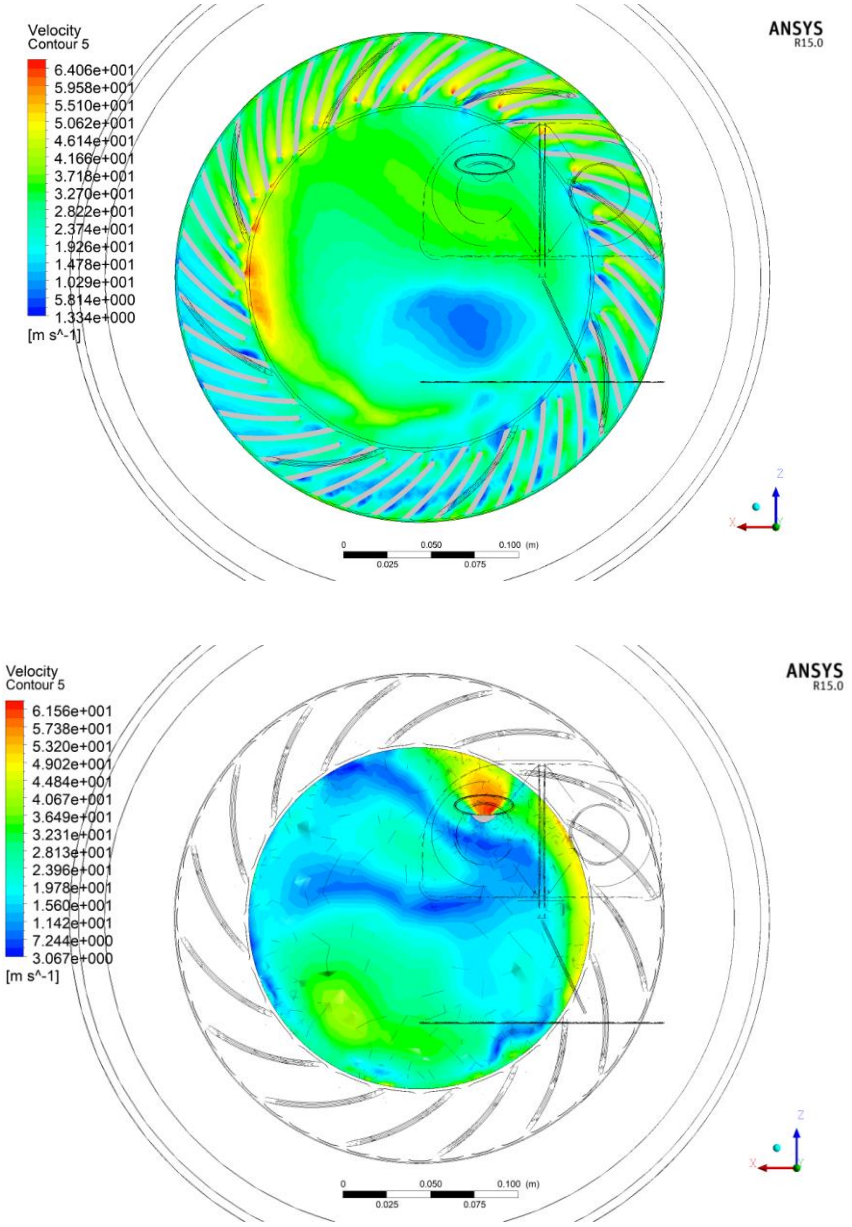

Figure 44 Duct with 70° angle and +25° flap.

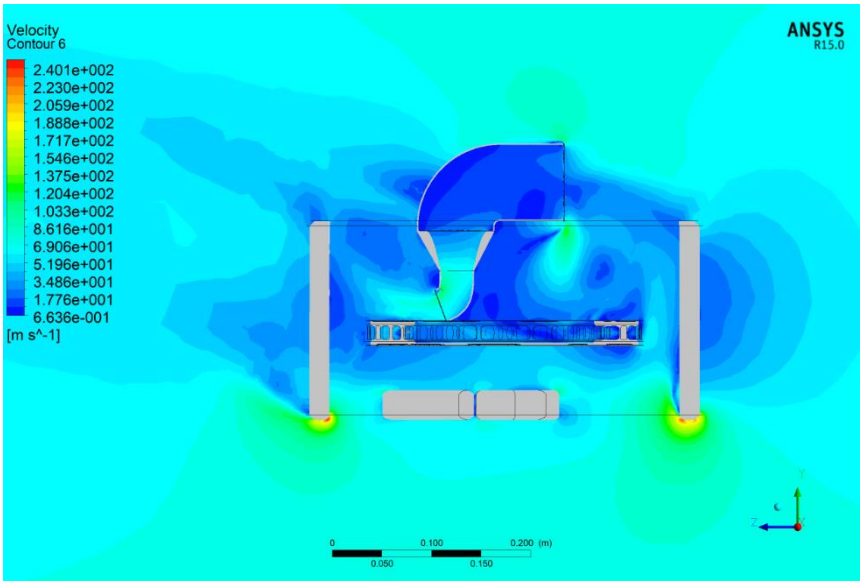

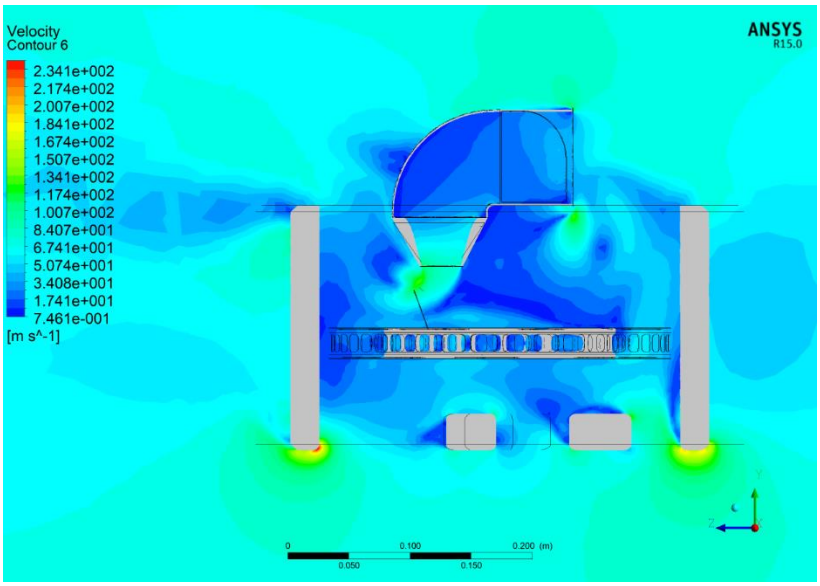

Figure 45 Bottom and Top duct outlet (70°, +25° flap).